molecules

MDPI

Article

Synthesis and In Vitro Anticancer Activity of Novel 4-Aryl-3-(4-methoxyphenyl)-1-phenyl-1*H*-pyrazolo[3,4-*b*]pyridines Arrest Cell Cycle and Induce Cell Apoptosis by Inhibiting CDK2 and/or CDK9

Basma S. Almansour [1], Faizah A. Binjubair [1], Alaa A.-M. Abdel-Aziz [1] and Sara T. Al-Rashood [1,*]

Department of Pharmaceutical Chemistry, College of Pharmacy, King Saud University, P.O. Box 2457, Riyadh 11451, Saudi Arabia; 443203434@student.ksu.edu.sa (B.S.A.); fbinjubair@ksu.edu.sa (F.A.B.); almoenes@ksu.edu.sa (A.A.-M.A.-A.)

* Correspondence: salrashood@ksu.edu.sa

Abstract: Two series of pyrazolo[3,4-*b*]pyridine derivatives, **9a–h** and **14a–h**, are synthesized and evaluated for their anti-cancer potency towards Hela, MCF7, and HCT-116 cancer cell lines. Compound **9a** showed the highest anticancer activity with IC_{50} = 2.59 μM against Hela when compared with doxorubicin (IC_{50} = 2.35 μM). Compound **14g** revealed cytotoxicity IC_{50} = 4.66 and 1.98 μM towards MCF7 and HCT-116 compared to doxorubicin with IC_{50} = 4.57 and 2.11 μM, respectively. Compound **9a** exhibited cell cycle arrest at the S phase for Hela, whereas **14g** revealed an arresting cell cycle for MCF7 at G2/M phase and an arresting cell cycle at S phase in HCT-116. In addition, **9a** induced a significant level of early and late apoptosis in Hela when compared with the control cells, whereas **14g** induced an apoptosis in MCF7 and HCT-116, respectively. Compounds **9a** (IC_{50} = 26.44 ± 3.23 μM) and **14g** (IC_{50} = 21.81 ± 2.96 μM) showed good safety profiles on normal cell line WI-38. Compounds **9a** and **14g** showed good inhibition activity towards CDK2, with IC_{50} = 1.630 ± 0.009 and 0.460 ± 0.024 μM, respectively, when compared with ribociclib (IC_{50} = 0.068 ± 0.004). Furthermore, **9a** and **14g** showed inhibitory activity towards CDK9 with IC_{50} = 0.262 ± 0.013 and 0.801 ± 0.041 μM, respectively, related to IC_{50} of ribociclib = 0.050 ± 0.003. Docking study for **9a** and **14g** exhibited good fitting in the CDK2 and CDK9 active sites.

Keywords: pyrazolo[3,4-*b*]pyridines; anti-cancer; cell cycle; apoptosis; CDK2; CDK9

Citation: Almansour, B.S.; Binjubair, F.A.; Abdel-Aziz, A.A.-M.; Al-Rashood, S.T. Synthesis and In Vitro Anticancer Activity of Novel 4-Aryl-3-(4-methoxyphenyl)-1-phenyl-1*H*-pyrazolo[3,4-*b*]pyridines Arrest Cell Cycle and Induce Cell Apoptosis by Inhibiting CDK2 and/or CDK9. *Molecules* **2023**, *28*, 6428. https://doi.org/10.3390/molecules28176428

Academic Editor: Antonio Palumbo Piccionello

Received: 25 June 2023
Revised: 11 July 2023
Accepted: 17 July 2023
Published: 4 September 2023

1. Introduction

Biomedical research has focused on how living cells grow and divide since the theory of spontaneous generation was disproved in the late seventeenth century, and the interest in the subject only increased as it became clear that sustained cellular proliferation was central to the initiation and progression of cancer, and today, sustained proliferative capacity is considered a hallmark of cancer [1]. Regulation of proliferation is defined by the work of Hartwell, Nurse, and Hunt, and they also defined the role of cyclin-dependent kinases (CDKs); hence, the 2001 Nobel Prize in Physiology and Medicine was awarded to them [2]. The cyclin-dependent protein kinases (CDKs) are protein-serine/threonine kinases that belong to the CMGC family (CDKs, mitogen-activated protein kinases, glycogen synthase kinases, and CDK-like kinases) [3]. The human genome encodes 21 CDKs, although only 7 (CDK 1, 2, 3, 4, 6, 10, 11) have a direct crucial role in the progression of the cell cycle, while other CDKs play an indirect role via activation of other CDKs (CDK 3), regulation of transcription (CDK7, 8, 9) or neuronal function (CDK 5). Different families of cyclins, the regulatory subunits required for CDK activity, have been identified, and their expression fluctuates significantly throughout the phases of the cell cycle [4]. CDK inhibitors may be used to treat cancer, diabetes, kidney disease, neurological illness, and infectious disease [5,6]. A variety of chemical classes, typically planar heteroaromatic

structures, such as flavonoid, purine, indenopyrazole, arylcarbazole, indolinone, oxindole, pyrimidine, thiazole, and indirubin, have been described as CDK inhibitors [7]. CDKs have been considered promising targets for the treatment of cancers and other diseases due to their crucial roles in the regulation of cell cycle and transcription. Since the 1990s, the first-generation CDK inhibitors have been explored [8]. These molecules include benzopyran derivative flavopiridol [9,10], imidazolo [4,5-*d*]pyrimidine roscovitine [11,12], and pyrazolo [1,5-*a*]pyrimidine dinaciclib (SCH-727965) [13,14] (Figure 1).

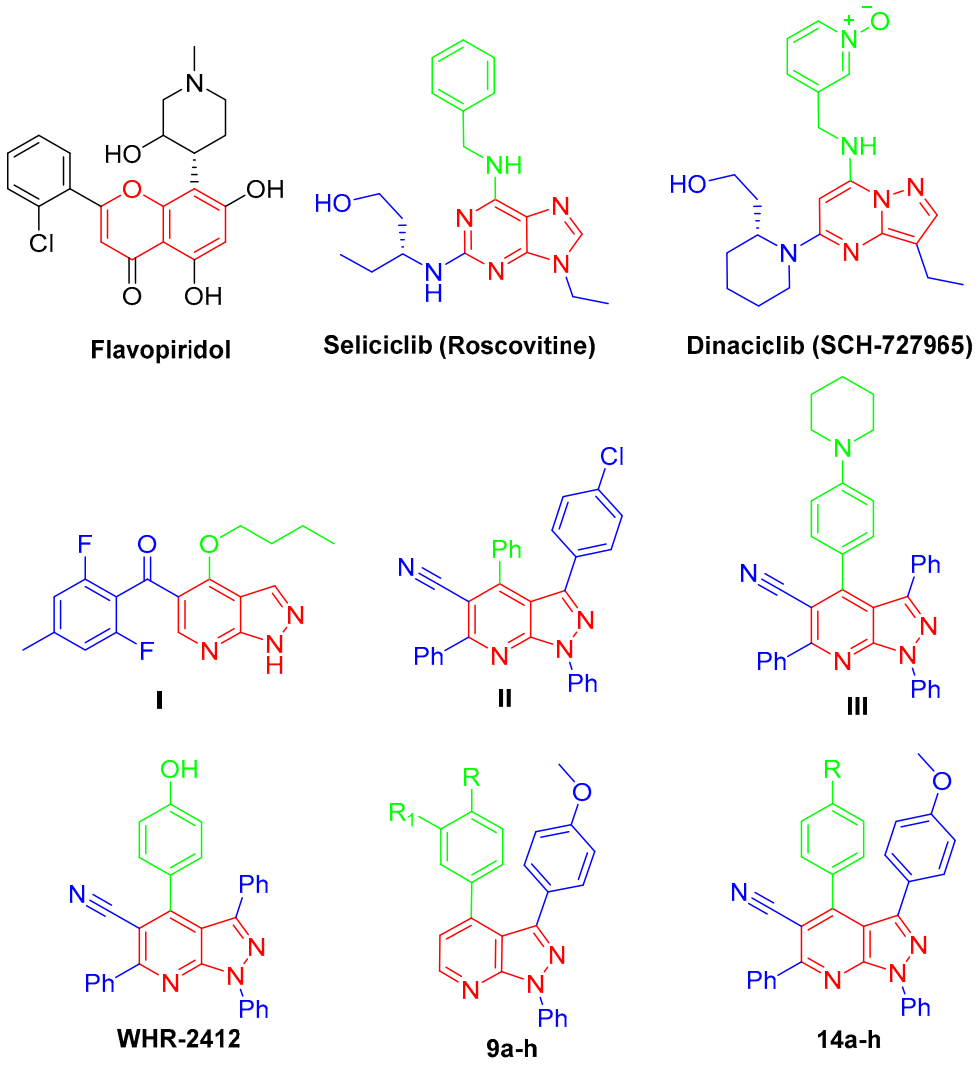

Figure 1. Chemical structures of flavopiridol, roscovitine, dinaciclib, pyrazolo[3,4-*b*]pyridines **I–III**, **WHR-2412**, and targeted compounds **9a–h** and **14a–h**.

In the last few decades, anticancer drugs have been developed from chemically synthesized compounds including pyrazole derivatives where their anticancer activity is due to the inhibition of various targets such as CDKs [15]. Important pyrazole-containing drugs were available in the market, such as Celecoxib, which showed very promising anticancer activity against prostate cancer cells [16,17]. On the other hand, pyridine derivatives serve as promising anticancer agents in the field; they acquired huge attention in current medicinal research due to their impact in curing numerous vicious ailments, such as breast cancer, myeloid leukemia, and idiopathic respiratory fibrosis [18,19]. Hybridization of pyrazole and pyridine scaffold is of great importance in cancer treatment, such as via sorafenib, regorafenib, vismodegib, and crizotinib. Pyrazolo[3,4-*b*]pyridine scaffold is an important central moiety of several anticancer agents, such as in the case of compounds **I–III** [20–23], which showed an interesting anti-cancer activity through different mechanisms, in addi-

tion to **WHR-2412**, which can exert its antitumor impact through CDK2 inhibition [24,25] (Figure 1).

There are three binding sites that have been reported in the CDK monomer: the ATP-competitive binding site (Site I) in addition to two non-competitive binding sites, II and III. Site I, the main target site of CDK2 inhibitors, has the impressive capacity to accommodate various ligands, including flat heterocyclic rings. On the other side, site III accommodates short peptide ligands, whereas the binding mechanism of Site II remains ambiguous. Furthermore, when CDK is subjected to the cyclin binding process, the resulting conformational changes give rise to a variation of the ATP binding site and then generate an allosteric binding site, i.e., Site IV, which requires the binding inhibitors to possess extraordinarily high inhibitory affinities. In precis, for designing potent CDK2 and CDK9 inhibitors, we can arrange the following principles: (1) developing inhibitors with flat heterocyclic rings for site I; (2) designing short peptide ligands for Site III; and (3) employing binding molecules which have extraordinarily high inhibitory affinities for Site IV [26,27].

In the light of the mentioned data, several drug design approaches were exploited in order to develop the target pyrazolo[3,4-*b*]pyridine derivatives, **9a–h** and **14a–h**, (Figure 2). First, the bioisosteric replacement strategy was utilized to replace the core heterocycle pyrazolo [1,5-*a*]pyrimidine in dinaciclib and imidazolo [4,5-*d*]pyrimidine core in roscovitine by the pyrazolo[3,4-*b*]pyridine core in the target structures. These fused heterocyclic are expected to be fitted into the ATP adenine binding pocket. Moreover, both roscovitine and dinaciclib are tethered with the hydroxyl functionality that is responsible for the hydrogen bonding. As a result, the methoxy functionality was grafted into the structure of our target compounds to ensure the requisite hydrogen bonding.

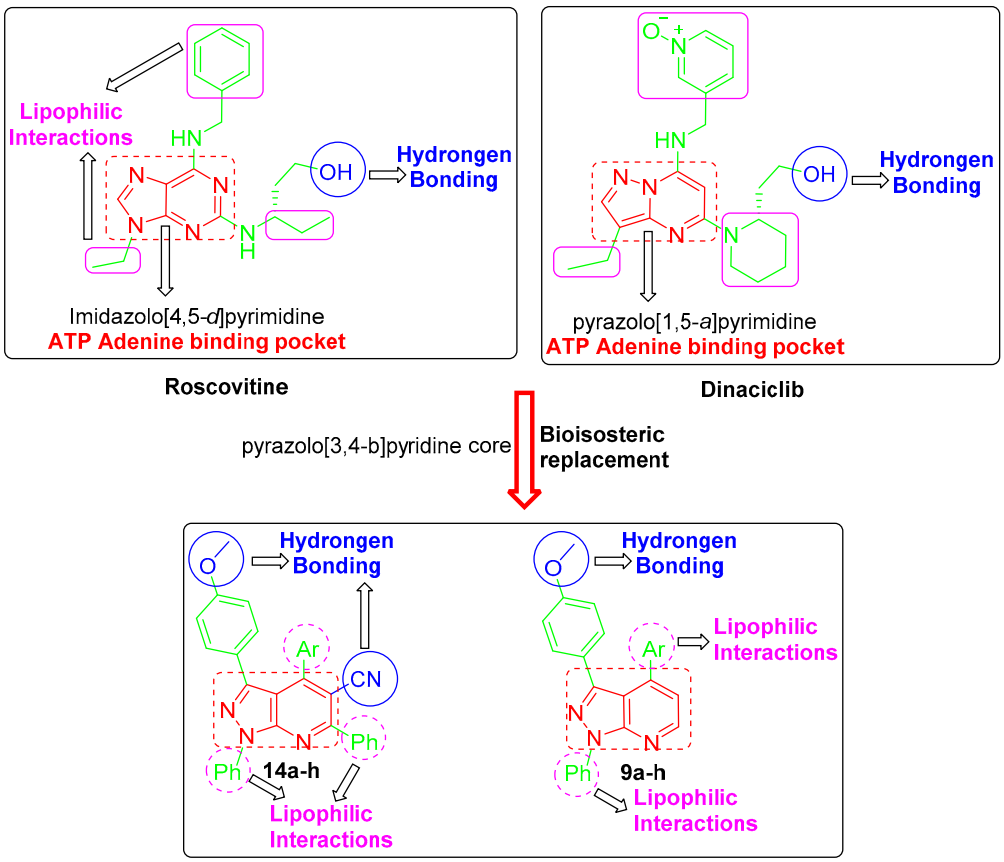

Figure 2. Design of the targeted pyrazolo[3,4-*b*]pyridine derivatives **9a–h** and **14a–h**.

Furthermore, the cyano functional group was incorporated in target compounds **14a–h** to enhance the hydrogen bonding interactions (Figure 2). Moreover, the target structures

were decorated with diverse lipophilic motifs to establish the required hydrophobic interactions within the CDK2 binding site. The variation of substitutions in **9a–h** and **14a–h** was adopted to provide different lipophilic environments (Figure 2). Interestingly, a pilot molecular modeling study showed a plausible binding mode and different interactions of the target molecules within their proposed target CDK2. As expected, a preliminary molecular modeling

study showed that the designed pyrazolo[3,4-*b*]pyridine derivatives **9a–h** and **14a–h** succeed in achieving the required hydrogen bonding and hydrophobic interactions.

2. Results and Discussion

2.1. Chemistry

3-(Phenyl/4-methoxyphenyl)-3-oxopropanenitrile **3a, b**, are prepared via the bromination of acetophenones **1a**, **b** to afford 2-bromo-1-(phenyl/4-methoxyphenyl)ethan-1-ones **2a**, **b**, followed by cyanation reaction (Scheme 1). Then, the key intermediate 3-(4-methoxyphenyl)-pyrazol-5-amine derivative **4b** is synthesized through the reaction of oxopropanenitrile **3b** with phenylhydrazine in refluxing ethanol (Scheme 1).

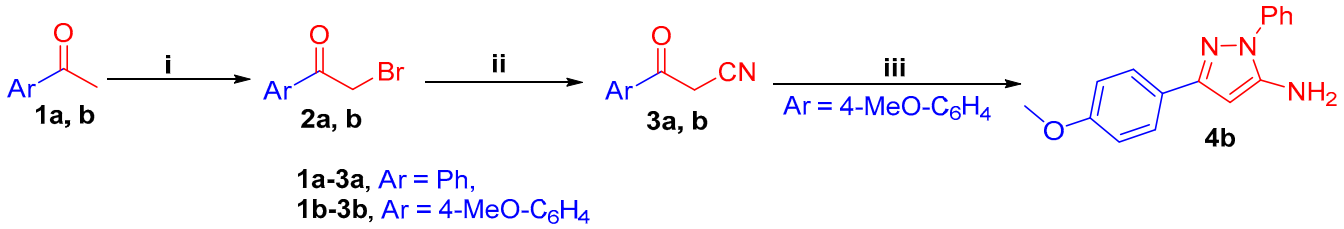

Scheme 1. (**i**) Br_2, AcOH, stirring, 1 h, rt; (**ii**) KCN, EtOH/H_2O, stirring, 2 h, rt; (**iii**) $PhNHNH_2$, EtOH, reflux, 6 h.

Amino pyrazole derivative **4b** reacted with prop-2-en-1-ones **6a–h**, which was prepared by the reaction of acetophenones **1a, b** with dimethylformamide-dimethylacetal (DMF-DMA) **5** in anhydrous xylene, to give 3-(4-methoxyphenyl)-pyrazolo[3,4-*b*]pyridines **9a–h**, respectively (Scheme 2). The latter reaction is proposed to proceed through *michael* addition of exocyclic NH_2 of amino pyrazole **4b** into the double bond of enaminones **6a–h** to form intermediate **7a–h**, which lost a dimethylamine molecule to give intermediate **7a–h**, which gave the final targeted compounds **9a–h** through an intramolecular cyclo-condensation reaction (Scheme 2).

The ^{1}HNMR of **9a–h** revealed the doublet signals of pyridine H_2 and H_3 around δ 8.60 and 8.00 *ppm*, respectively, with coupling constant (*J*) around 6.5 Hz. ^{1}HNMR of **9a–h** showed the singlet signal of the methoxy group of the pyrazole 4-methoxyphenyl group around δ 3.87 *ppm*, whereas compounds **9b** and **9c** revealed an additional signal of methyl and methoxy groups at δ 2.41 and 3.855 *ppm*, respectively. Moreover, the signals of two methoxy groups of **9h** appeared at δ 3.86 and 3.93 *ppm*, respectively. ^{13}CNMR of **9a–h** showed the signals of pyrazole aryl –$\underline{C}H_3$O-C_6H_4 carbon at δ 55.75 *ppm*, in addition to the signals of SP^3 carbons of pyridine aryl for –$\underline{C}H_3$-C_6H_4 in **9b**, –$\underline{C}H_3$O-C_6H_4 in **9c** and *para* and *meta*–$\underline{C}H_3$O-C_6H_3 in **9h** at δ 21.38, 55.79, 55.90, and 56.07 *ppm*, respectively.

On the other side, one-step three components reaction of pyrazol-5-amine **4b**, 3-oxo-3-phenylpropanenitrile (**3a**) and the aromatic aldehydes **10a–h** give pyrazolo[3,4-*b*]pyridine-5-carbonitriles **14a–h**, respectively (Scheme 3). The IR of **14a–h** appeared as the characteristic sharp band of C≡N at 2218–2226 cm^{-1}. ^{1}HNMR of **14a–h** exhibited the singlet signal of the methoxy group of the pyrazole 4-methoxyphenyl group around δ 3.72–3.76 *ppm*. The ^{1}HNMR of **14g** showed the D_2O exchangeable signal of -O$\underline{H}$ as a broad singlet at δ 9.90 *ppm*, whereas the ^{1}HNMR of **14f** showed the signal of two methyl groups of -N(Me) as one singlet with integration equal to 6 protons at δ 2.93 *ppm*. The latter reaction proceeded via the condensation reaction between 3-oxo-3-phenylpropanenitrile (**3b**) and aldehydes **10a–h**, then the addition of H4 of pyrazole to give intermediate **11a–h**. The intramolecular

cyclocondensation of **11a–h** gives the target pyrazolo[3,4-*b*]pyridine derivatives **14a–h**, respectively (Scheme 3).

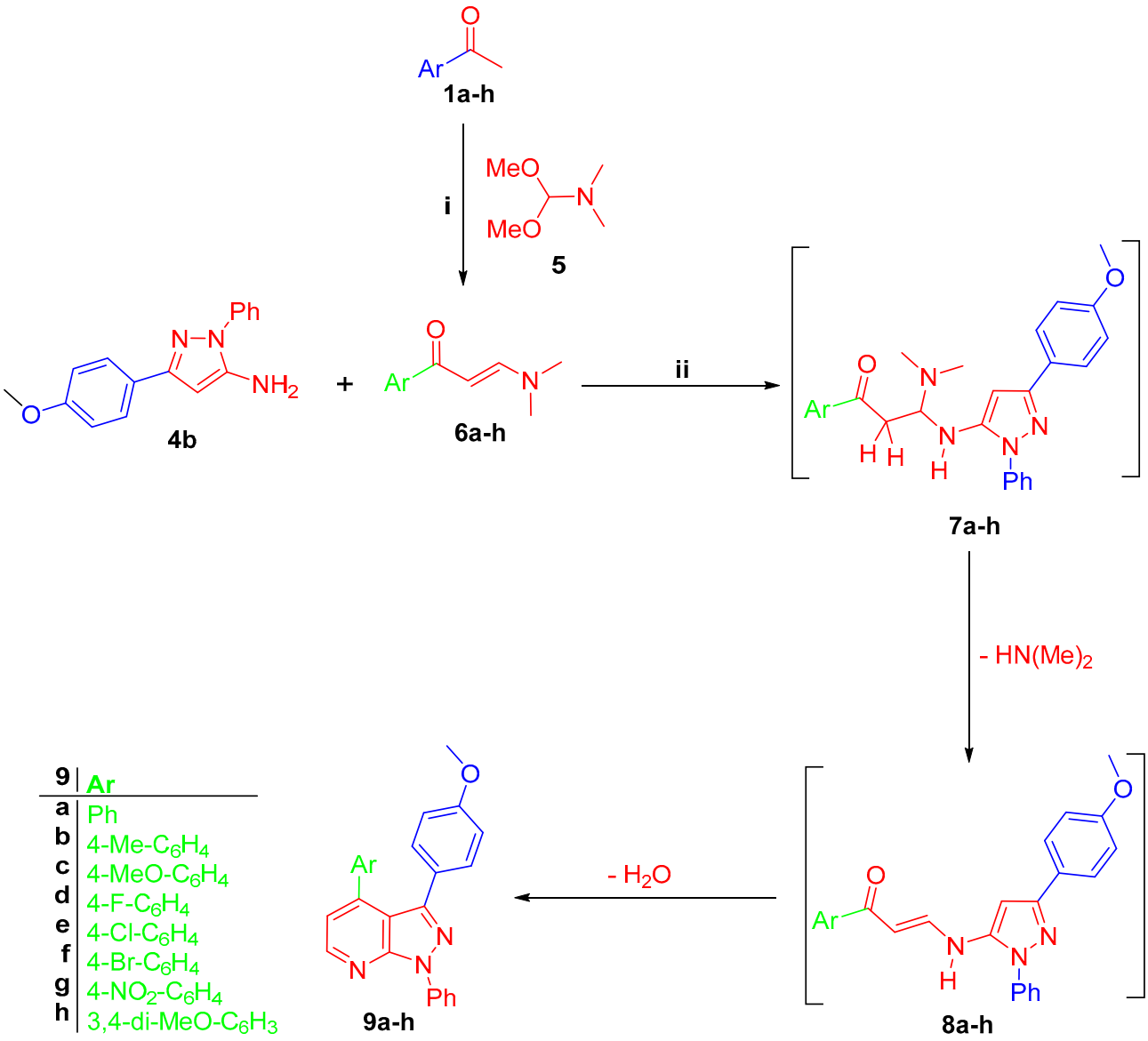

Scheme 2. (**i**) DMF-DMA, anhydrous xylene, reflux 8 h; (**ii**) glacial AcOH, refluxed for 4–6 h.

2.2. Biological Evaluation

2.2.1. Anti-Cancer Activity of **9a–h** and **14a–h** against Hela, HCT-116, and MCF7 Cancer Cell Lines

The cytotoxicity of compounds **9a–h** and **14a–h** against three cell lines, namely, cervical cancer Hela, breast cancer MCF7, and colon HCT-116, compared with doxorubicin as a reference compound was performed using MTT assay. The cytotoxic concentration (IC_{50} in μM) is illustrated in Table 1. Among the screened compounds, **9a** and **14g** showed significant anticancer activity. Compound **9a** showed the highest anticancer activity, with IC_{50} = 2.59 μM against Hela cell lines when compared with doxorubicin (IC_{50} = 2.35 μM) (Table 1). Compounds **14g** revealed cytotoxicity IC_{50} = 4.66 and 1.98 μM towards MCF7 and HCT-116 cell lines compared to doxorubicin with IC_{50} = 4.57 and 2.11 μM, respectively (Table 1).

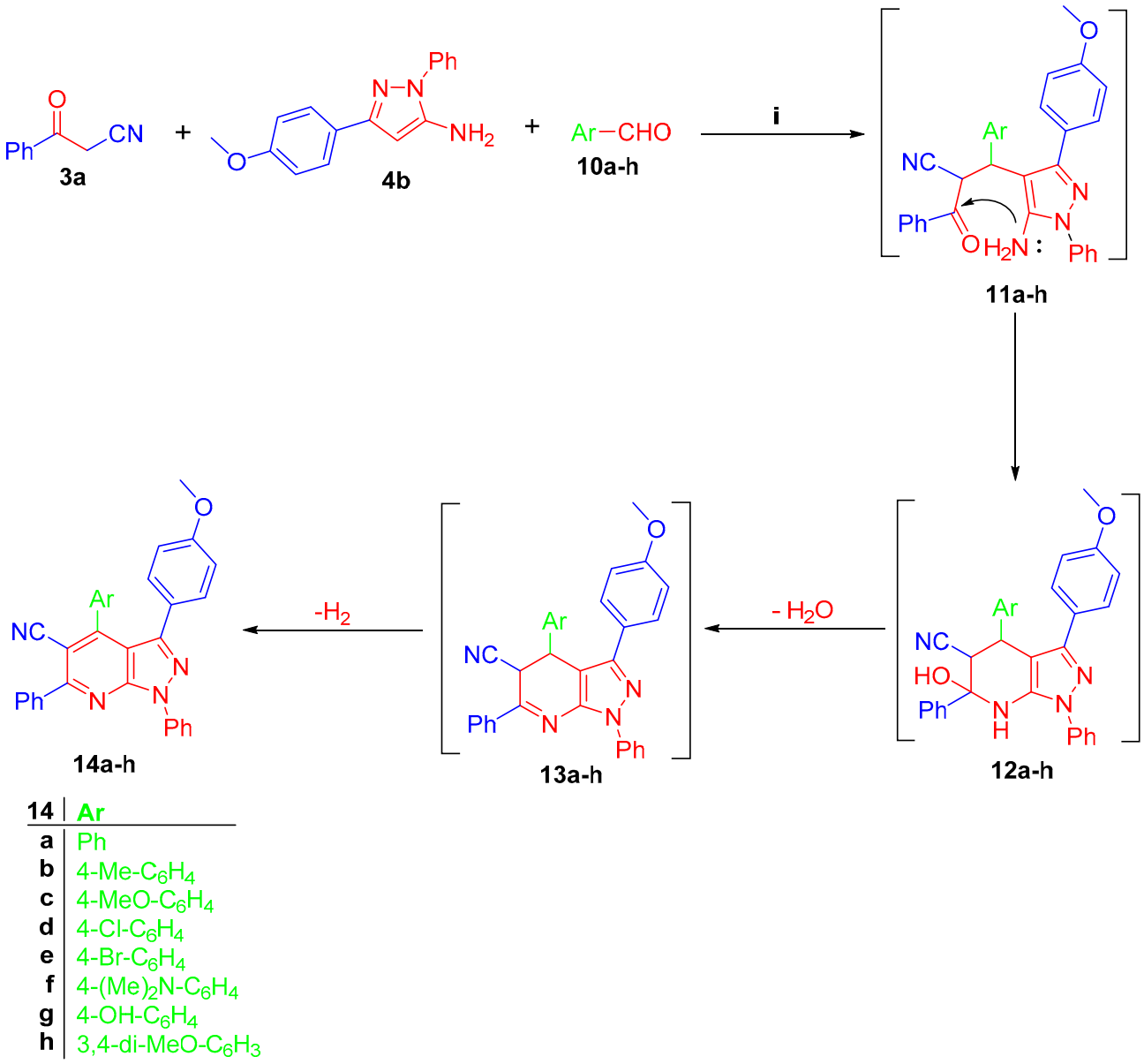

Scheme 3. (**i**) EtOH, TEA (catalytic), reflux 6–10 h.

2.2.2. SAR Studies

The potent anticancer activity of compounds **9a** and **14g** exhibited the impact of the electronic characteristics of substitution phenyl in position 4 of the pyridine ring with respect to its substituents in the *para* position. In compounds **9a**–**h**, these substitutions in **9b**–**h** gave low anticancer activity when compared with *para*-unsubstituted phenyl in **9a** with respect to Hela cell line. The 3,4-dimethoxyphenyl in **9h** improves the anticancer activity against Hela cell line when compared with **9b**–**f**, but it is still less than that of **9a**. Compound **14g**, with *para*-hydroxy substitution in the same phenyl ring, showed the highest anticancer activity against Hela among series **14a**–**h** but still less than the standard reference drug. Compound **14g**, with OH group in the phenyl group of position 4 in pyridine moiety, in addition to the Ph group in position 2 and the CN function in position 3 of the pyridine moiety, enhanced its anticancer activity towards MCF7 and HCT-116 cell lines. In the light of previous data, it can be noticed that the pyrazolo[3,4-*b*]pyridine system in compounds **9a**–**h** and **14a**–**h,** in addition to the substitutions around it, are necessary for their anticancer activity.

Table 1. Anticancer activity of **9a–h** and **14a–h** against MCF7, HCT-116, and Hela cancer cell lines.

Compound	IC50% μM		
	Hela	MCF7	HCT116
9a	2.59 ± 0.16	6.39 ± 0.46	15.26 ± 1.46
9b	13.96 ± 1.25	22.35 ± 3.18	18.01 ± 1.16
9c	26.63 ± 3.37	59.04 ± 5.52	43.17 ± 3.26
9d	19.59 ± 1.68	13.01 ± 1.33	17.46 ± 0.98
9e	48.45 ± 4.20	20.31 ± 3.21	16.58 ± 1.34
9f	20.44 ± 1.74	35.56 ± 4.64	16.78 ± 0.76
9g	28.26 ± 4.23	26.28 ± 2.85	40.02 ± 3.19
9h	7.92 ± 1.11	9.70 ± 1.00	9.69 ± 0.56
14a	23.05 ± 1.63	20.72 ± 1.73	25.82 ± 2.58
14b	20.98 ± 2.18	21.39 ± 2.05	36.29 ± 1.83
14c	41.27 ± 2.79	39.34 ± 3.74	36.73 ± 2.02
14d	21.07 ± 2.03	37.21 ± 2.48	31.14 ± 3.54
14e	37.33 ± 3.32	34.36 ± 2.59	37.77 ± 2.63
14f	46.14 ± 3.70	19.56 ± 1.26	39.96 ± 4.32
14g	12.65 ± 1.53	4.66 ± 0.38	1.98 ± 0.17
14h	31.69 ± 2.48	38.12 ± 2.76	3.69 ± 0.11
Doxorubicin	2.35 ± 0.08	4.57 ± 0.28	2.11 ± 0.20

Data are presented as the mean of the IC_{50} values ± SD from three different experiments.

2.2.3. Cell Cycle and Apoptosis

Cell Cycle

Cell cycle arrest of cervical cancer cells Hela, breast cancer cells MCF7, and colon cancer cells HCT-116 were assessed for compounds **9a** and **14g** at their IC_{50}. Compound **9a** exhibited high cell accumulation (29.54%, 1.23 fold) for the Hela cell line at the S phase (Control; 24.11%) that signifies cell cycle arrest at the S phase (Table 2, Figures 3 and 4). Compound **14g** exhibited cell cycle arrest for breast cell line MCF7 at G2/M—the phase with DNA accumulation, 24.94%, (1.68 fold), compared with the control, 14.86% (Table 2, Figures 2 and 3). In addition, the compound **14g** arresting cell cycle at S phase in HCT-116 cell lines with cell accumulation = 34.82% (1.97 fold) when compared with the control cells (17.64%) (Table 2, Figures 3 and 4).

Table 2. Cell cycle analyses for compounds **9a** and **14g** against MCF7, HCT-116, and Hela cancer cell lines.

Compound/Cell Line	DNA Content			Comment
	%G0-G1	%S	%G2/M	
9a/Hela	59.1	29.54	11.36	cell growth arrest@ S
Hela control	61.39	24.11	14.5	---
14g/MCF7	41.25	33.81	24.94	cell growth arrest@ G2/M
MCF7 control	46.12	39.02	14.86	---
14g/HCT-116	51.94	34.82	13.24	cell growth arrest@ S
HCT-116 control	55.87	26.49	17.64	---

Apoptosis Assay

An apoptotic assay using Annexin V/PI analysis for compounds **9a** and **14g** is evaluated. Compound **9a** induced a significant level of early and late apoptosis (total = 42.19) in the Hela cell line when compared with the control cells (Table 3, Figures 5 and 6). Compound **14g** revealed total apoptosis = 22.89 and 26.71 in MCF7 and HCT-116 cell lines, respectively, compared with the control cells (Table 3, Figures 5 and 6).

Table 3. Apoptosis analysis for **9a** and **14g** against MCF7, HCT-116, and Hela cancer cell lines.

Compound	Apoptosis			Necrosis
	Total	Early	Late	
9a/Hela	42.19	23.21	12.82	6.16
Hela control	2.33	0.49	0.12	1.72
14g/MCF7	22.89	13.07	7.55	2.27
MCF7 control	1.49	0.44	0.27	0.78
14g/HCT-116	26.71	16.01	6.95	3.75
HCT-116 control	2.51	0.63	0.19	1.69

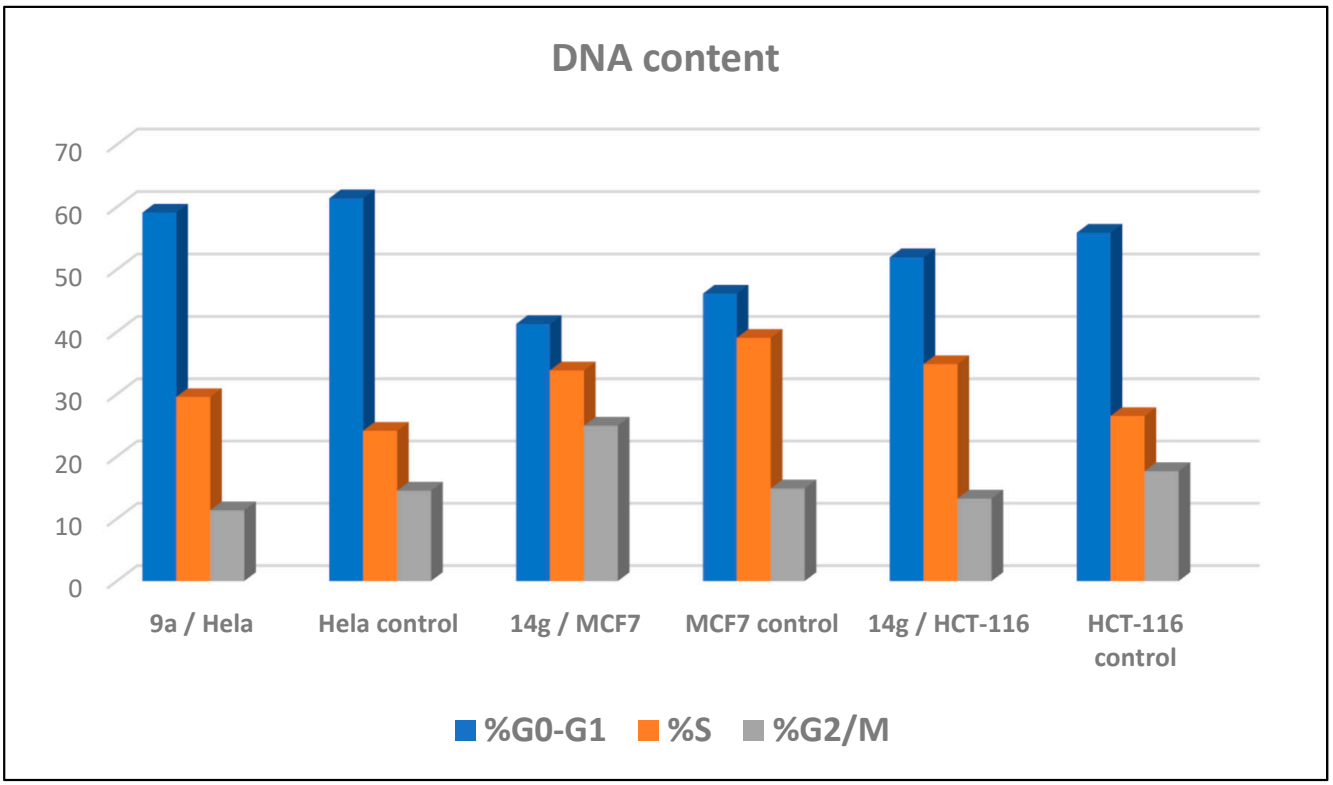

Figure 3. Representative diagram for cell cycle analyses for **9a** against Hela and **14g** against MCF7 and HCT-116, respectively.

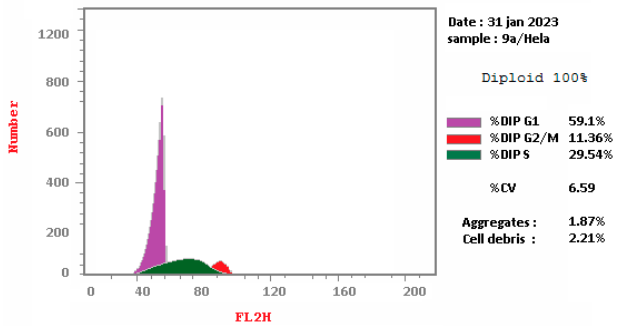

9a/Hela

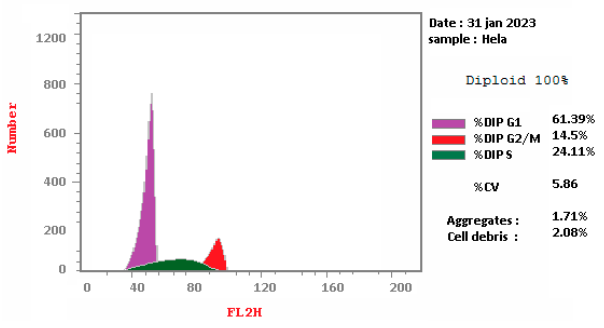

Hela

Figure 4. *Cont.*

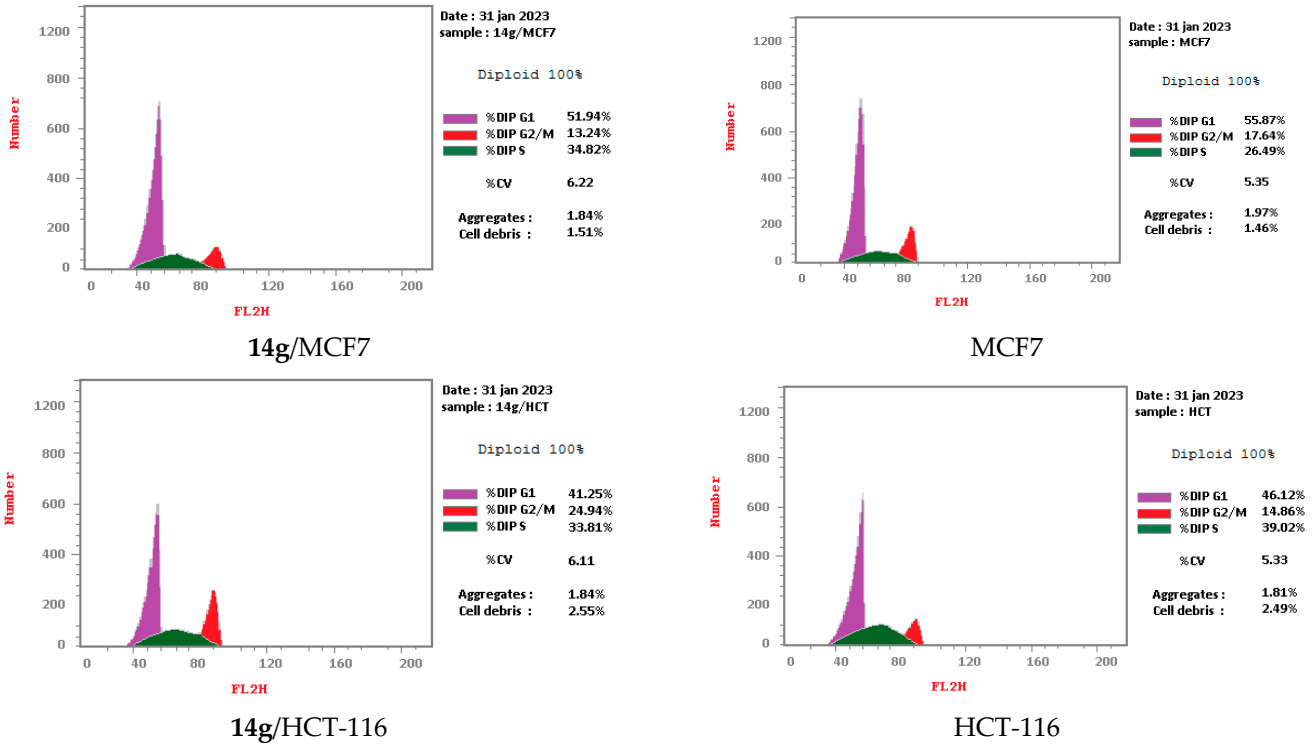

Figure 4. Cell cycle analyses for **9a** against Hela and **14g** against MCF7 and HCT-116, respectively.

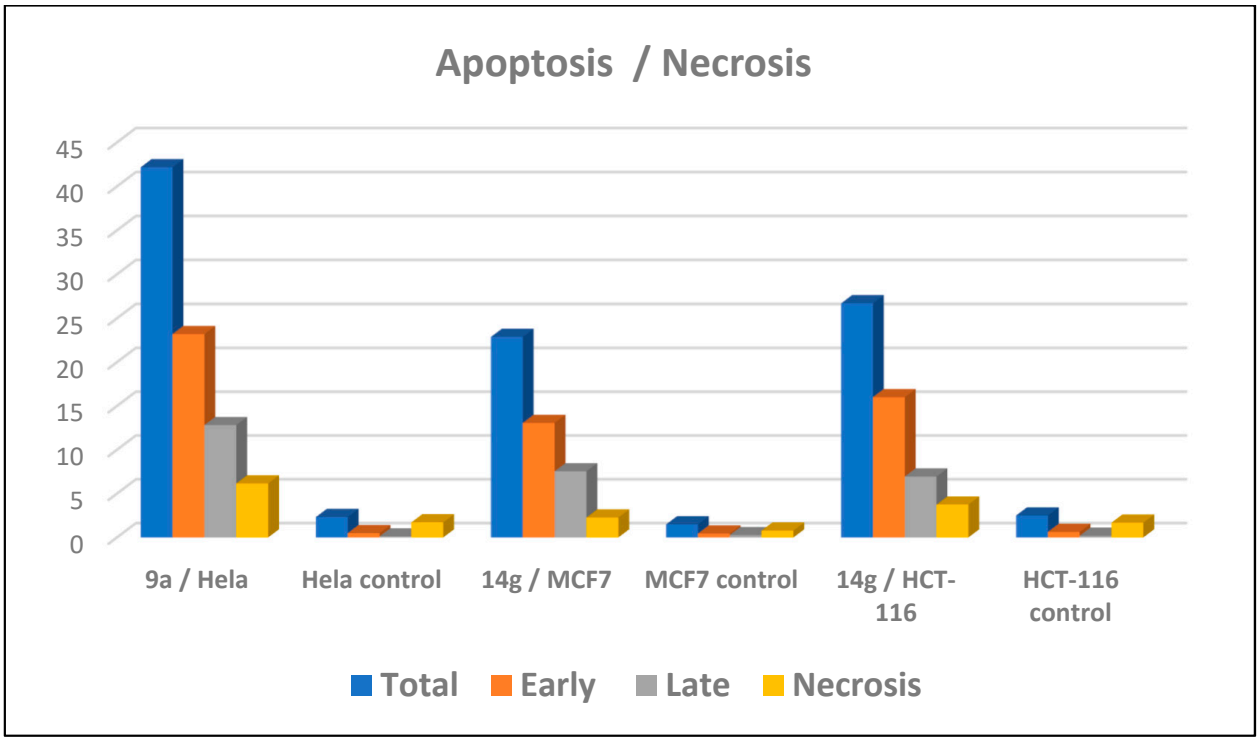

Figure 5. Representative diagram for apoptosis analyses for **9a** against Hela and **14g** against MCF7 and HCT-116, respectively.

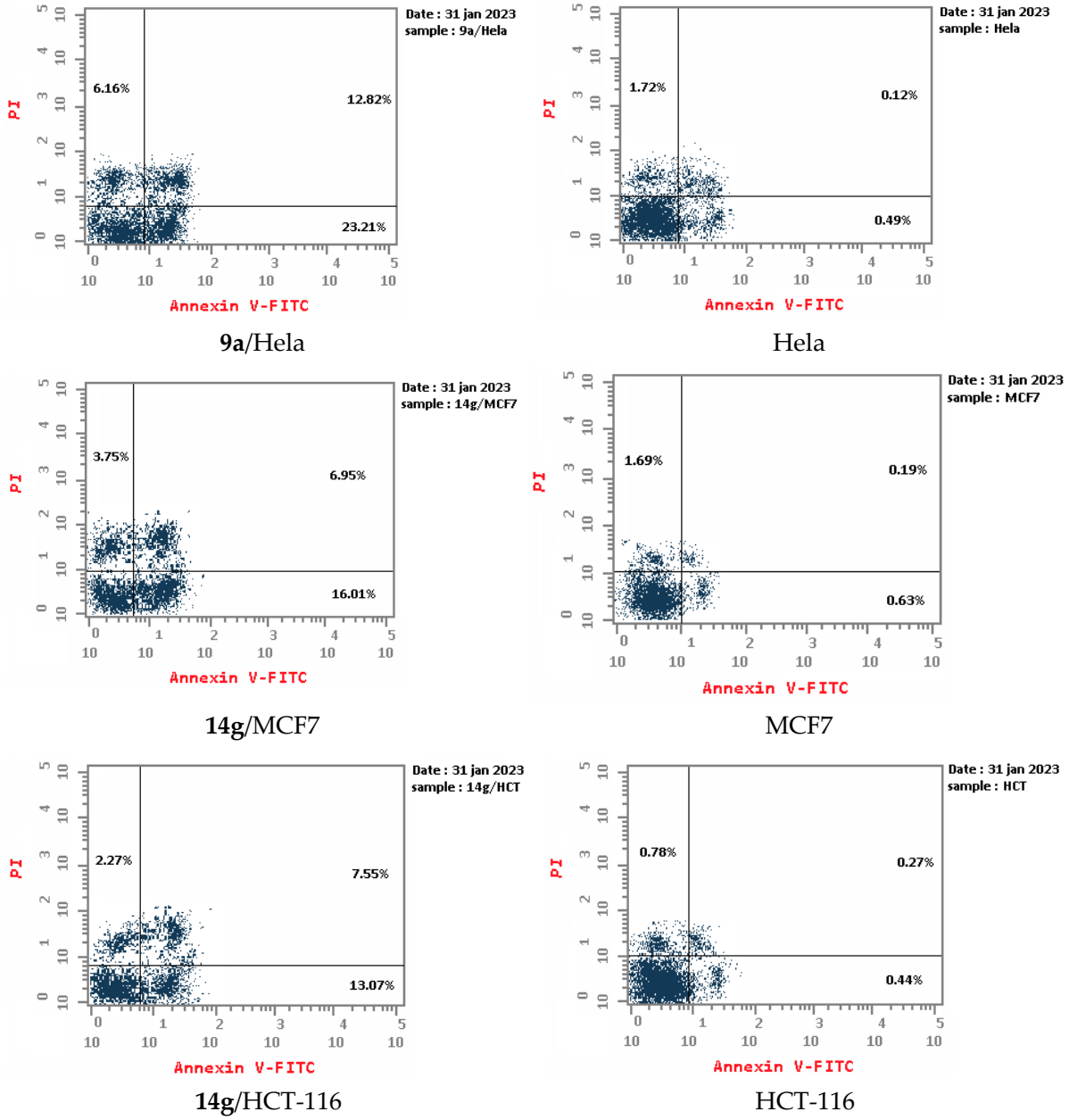

Figure 6. Apoptosis analyses for **9a** against Hela and **14g** against MCF7 and HCT-116, respectively.

2.2.4. Cytotoxicity of **9a** and **14g** on Normal Cell Line

The cytotoxicity of the most effective compounds **9a** and **14g** towards human normal cell line WI-38 was evaluated comparing with doxorubicin as a reference drug using MTT assay. Compounds **9a** (IC_{50} = 26.44 ± 3.23 μM) and **14g** (IC_{50} = 21.81 ± 2.96 μM) showed good safety profiles on normal cell line WI-38 when compared with doxorubicin (IC_{50} = 15.60 ± 0.37 μM) (Table 4).

Table 4. In vitro anticancer activities of **9a** and **14g** against human normal WI-38 cells.

Compound	In Vitro Cytotoxicity on WI-38 (IC_{50}, μM) [a]
9a	26.44 ± 3.23
14g	21.81 ± 2.96
Doxorubicin	15.60 ± 0.37

[a] Data are presented as the mean of the IC_{50} values ± SD from three different experiments.

2.2.5. CDK2 and CDK9 Enzyme Assay Inhibition of **9a** and **14g**

The in vitro CDK2 and CDK9 inhibitory activity of **9a** and **14g** was assayed using ribociclib as a standard CDK inhibitor, and their IC_{50} (μM) are illustrated in Table 5. Compounds **9a** and **14g** showed good inhibition activity towards CDK2 with IC_{50} = 1.630 ± 0.009 and 0.460 ± 0.024 μM, respectively, when compared with ribociclib (IC_{50} 0.068 ± 0.004). Furthermore, compounds **9a** and **14g** showed inhibitory activity towards CDK9 with IC_{50} = 0.262 ± 0.013 and 0.801 ± 0.041 μM, respectively, related to IC_{50} of ribociclib = 0.050 ± 0.003.

Table 5. CDK2 and CDK9 inhibitory activity ($IC_{50,}$ μM) for **9a**, **14g** and ribociclib.

Compound	IC_{50} (μM)	
	CDK2	**CDK9**
9a	1.630 ± 0.009	0.262 ± 0.013
14g	0.460 ± 0.024	0.801 ± 0.041
Ribociclib	0.068 ± 0.004	0.050 ± 0.003

2.3. Molecular Modeling

A molecular docking study on compounds **9a** and **14g** in the active site of CDK2 and CDK9 enzyme to correlate the in vitro *enzyme* activity with their binding mode with enzymes' active sites using the molecular operating environment (MOE) 2019.02 and 3D coordinates of CDK2 and CDK9 (PDB IDs 3tnw and 3tn8 with resolution 2 and 2.95 Å, respectively). Valid docking protocol is established through the complexing of CDK2 and CDK9 with CAN508 as a potent CDK inhibitor with 0.265 and 0.4337 Å (Figure 7). The interaction modes of the ligand with the active sites should not be only determined as the highest energy scored protein–ligand complex used during docking but also bears in mind the conformers of each compound which are mostly associated with bioactive conformations. Based on the binding free energies and their correlation with the inhibitory activities, we can give a more quantitative explanation of the structure–activity relationship of the inhibitory mechanism for these compounds [28–30]. The output of the docking simulation is the scoring function which reflects the binding free energy dG in Kcal/mol. This step showed an energy score of −11.7195 and −10.045 kcal/mol for CAN508 in CDK2 and CDK9, respectively.

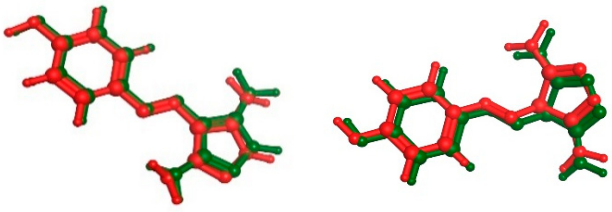

(**A**) (**B**)

Figure 7. The superimposition of co-crystallized (red) and docking pose (green) of CAN508 in CDK2 (**A**) and CAN508 in CDK9 (**B**) active sites.

2.3.1. Docking of **9a** and **14g** in CDK2 Binding Site

The binding of CAN508 with CDK2 active site showed the formation of two H-bonds with Asp145 and Leu83 residues, and two pi–H bonds with Val18 and Leu134 (Figure 8A). Docking simulations for **9a** and **14g** exhibited a good fit in the CDK2 active site with docking scores −13.0738 and −14.924 kcal/mol, respectively, when compared with that of CAN508 (−11.7195 kcal/mol). The higher binding free energy of **9a** and **14g**, compared with CAN508, explained their good affinity to CDK2 active site. The binding patterns of **9a** (Figure 8B) and **14g** (Figure 8C) are consistent with the crystallographic binding of CAN508 in the CDK2 active site.

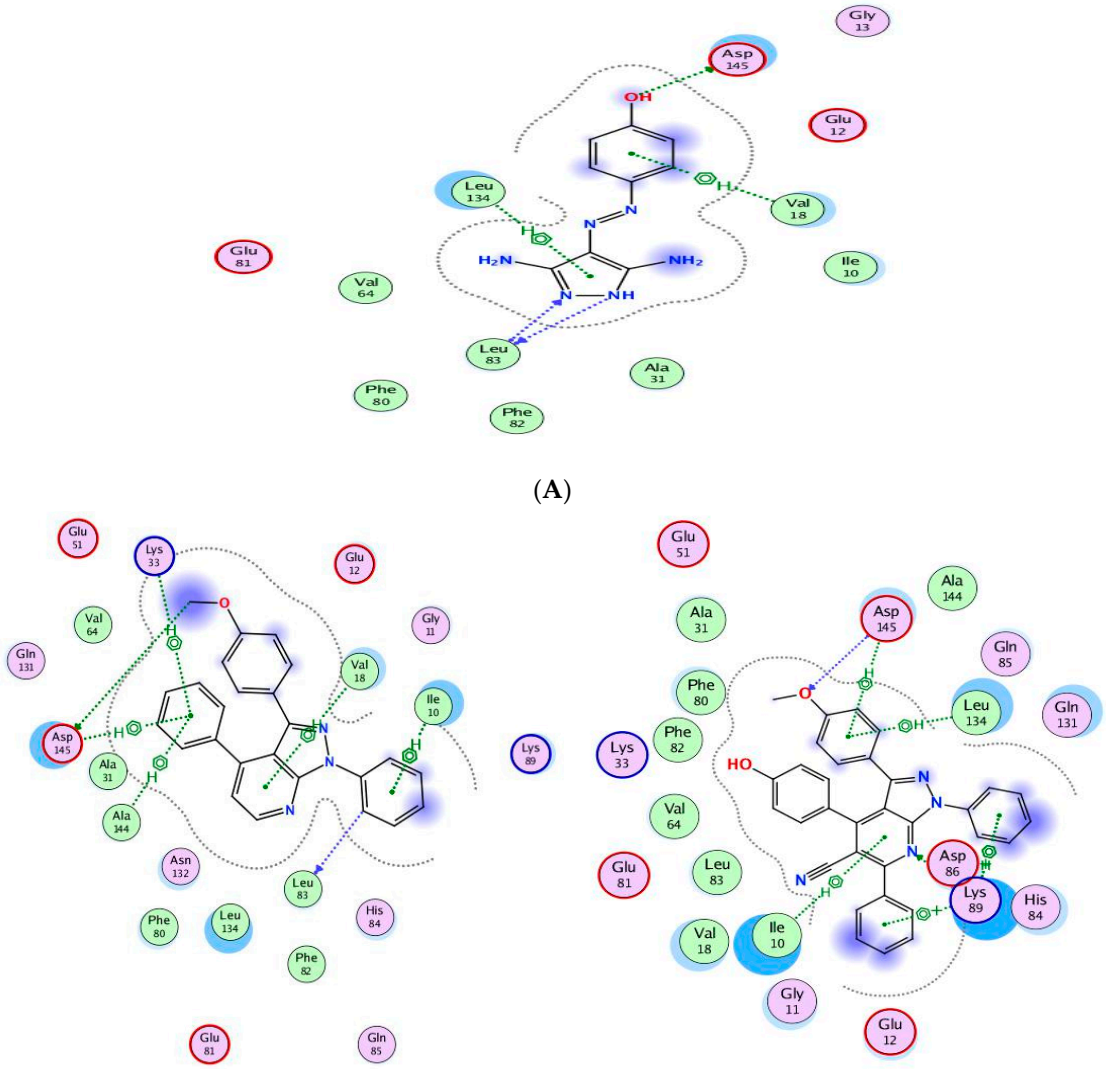

Figure 8. Two-dimensional binding interactions of CAN508 (**A**), **9a** (**B**), and **14g** (**C**) in the CDK2 binding site in which green arrows represent H-bond interaction in the sidechain, blue arrows represent H-bond interaction in the backbone, the benzene/H structure on the green bond represents pi–hydrogen interactions, and the benzene/+ structure on the green bond represents pi–cation interactions.

For example, the methoxy group in the phenylmethoxy ring of both compounds **9a** and **14g** was H-bonded with the key residue Asp145. The latter H-bond highlighted the important role of the methoxy group of the phenyl ring in these compounds in CDK9 inhibition. Moreover, binding with Asp145 by pi–hydrogen bond through the phenyl ring of pyridine in **9a** and the phenylmethoxy ring in **14g** are noticed. Both compounds bind with Ile10 by pi–hydrogen bond through a phenyl ring attached to pyrazole in compound **9a** and the pyridine ring in compound **14g**. Compound **9a** binds the key residue Leu83 by a hydrogen bond through its phenyl ring attached to pyrazole. Further pi–hydrogen interactions are observed between compound **9a** and Val18, Lys33 and Ala144 (Figure 9A). Compound **14g** is anchored by the key residue Lys89 by hydrogen, pi–cation, and pi–hydrogen bonds. Further pi–hydrogen interaction between compound **14g** and Leu134 is observed (Figure 9B).

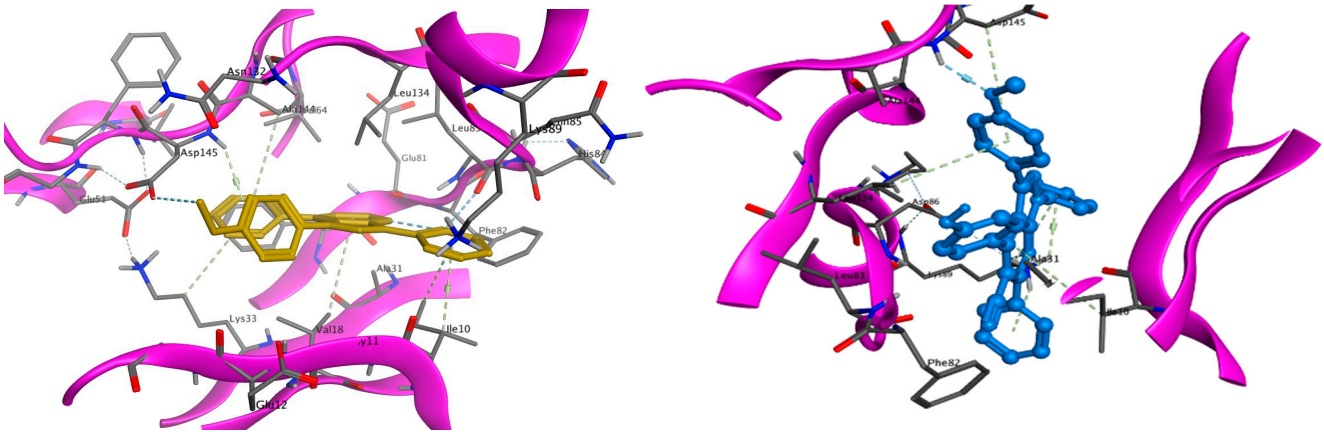

(**A**) (**B**)

Figure 9. Binding interactions (3D diagram) for **9a** (**A**) and **14g** (**B**) in the CDK2 binding site.

2.3.2. Docking of **9a** and **14g** in CDK9 Binding Site

Compounds **9a** and **14g** showed good docking scores with high free binding energy (−10.6742 and −10.1599 kcal/mol) compared to CAN508 (−10.045 kcal/mol). Figure 10A shows that CAN508 formed an H-bond with the Lys48 residue and a pi–hydrogen interaction with Val33 in the CDK9 active site. Interestingly, **9a** and **14g** revealed essential interactions in CDK9 active sites (Figure 10B,C). For instance, both compounds formed an H-bond with essential key residue Lys48 via the oxygen atom of the phenylmethoxy ring. This illustrates the importance of additional methoxy group in our compounds. The phenyl ring attached to pyrazole forms a hydrogen bond with the key residue Ala153 in both compounds. Both compounds form pi–hydrogen interactions leu156 and Ile25 via pyrazole and pyridine rings, respectively, noting that there is an additional interaction in compound **14g** via the phenyl group of the pyridine ring and this explains the stronger binding and score in this compound.

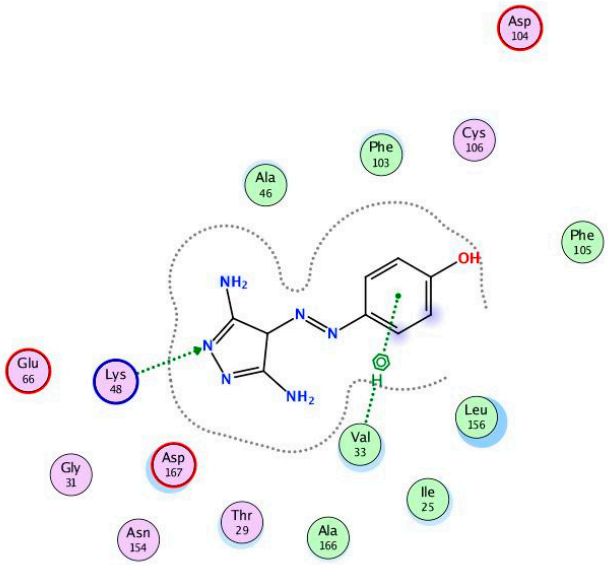

(**A**)

Figure 10. *Cont.*

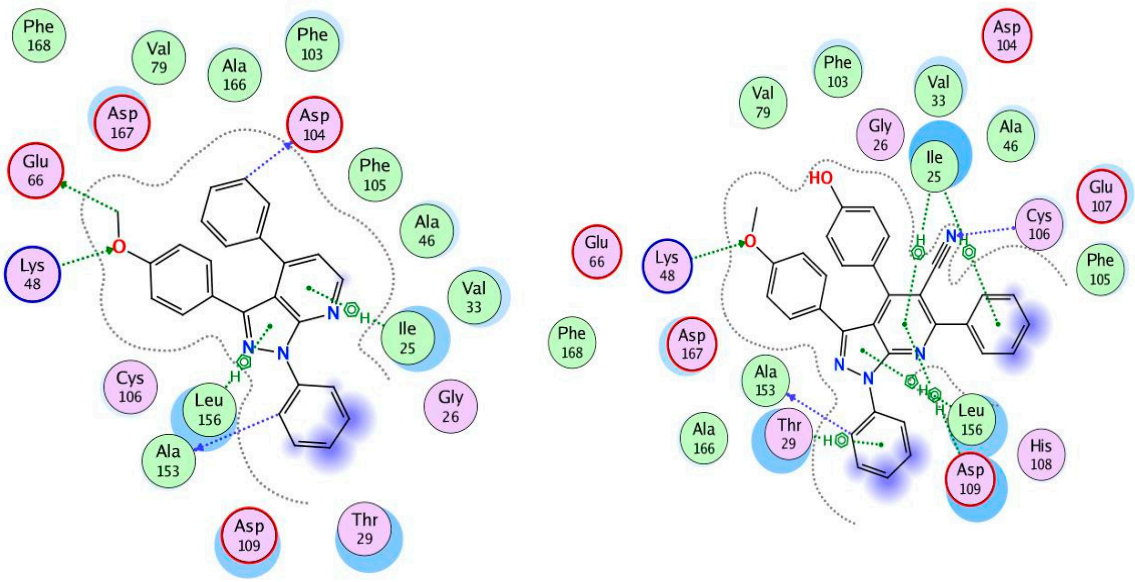

(**B**) (**C**)

Figure 10. Binding interactions (2D diagram) for CAN508 (**A**), **9a** (**B**), and **14g** (**C**) in the CDK9 binding site in which green arrows represent H-bond interaction in the sidechain, blue arrows represent H-bond interaction in the backbone, and the benzene/H structure on the green bond represents pi–hydrogen interactions.

Compound **9a** forms two hydrogen bonds with Glu66 and Asp104 via the methoxy group and phenyl ring attached to pyridine, respectively. Compound **14g** forms a hydrogen bond with the key residue Cys106 via the nitrogen atom in the nitrile group in addition to two pi–hydrogen interactions with Asp104 and Leu156 (Figure 11A,B).

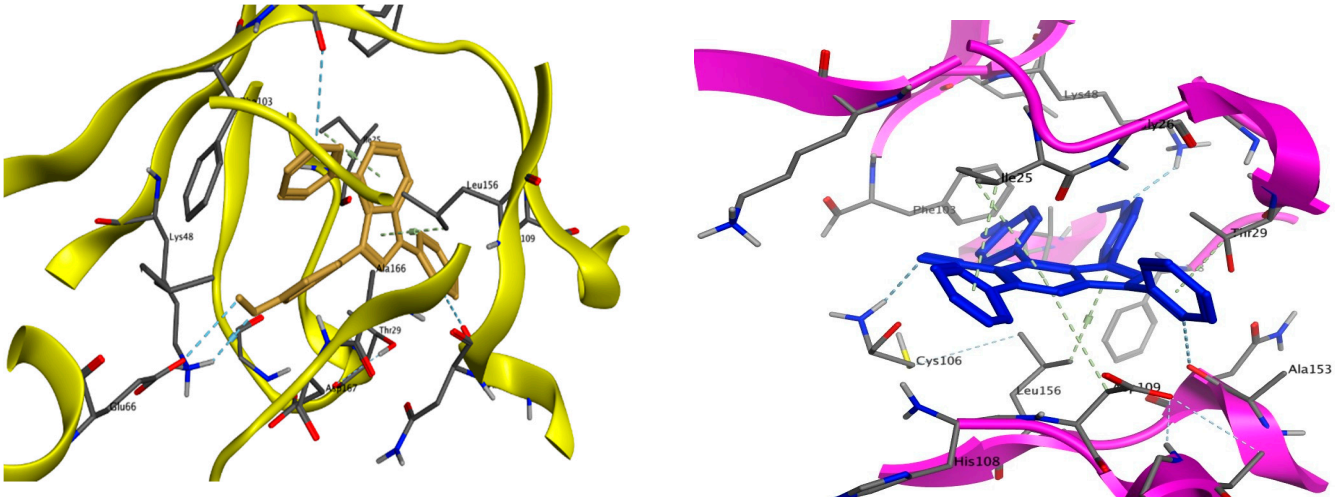

(**A**) (**B**)

Figure 11. Binding interactions (3D diagram) of **9a** (**A**) and **14g** (**B**) in the CDK9 binding site.

3. In Silico ADME Study

A small molecule's therapeutic activity is determined by its ability to reach the aimed target at a sufficient concentration, which can be determined by its ADME properties. Lipinski's rule-of-five states if a small molecule has the potential to be a medication. SwissADME provides rapid but reliable prediction data about a small molecule's physicochemical parameters (such as molecular weight, partition coefficient, solubility, topological surface area, and so on), as well as pharmacokinetics and drug likeness [31,32]. This method may fore-

cast lead molecules with desired drug-like features and can be used to change or improve a molecule such that it has all desirable lead-like or drug-like properties. As a result, we employed the SwissADME model to forecast the properties of our newly created molecules **9a**–**h** and **14a**–**h**. According to the data gathered from this web tool, all compounds obey the Veber rule (Table 6) with zero violations indicating their drug-likeliness.

Table 6. SwissADME prediction of physicochemical properties and bioavailability of **9a**–**9h** and **14a**–**h**.

Compound	Fraction Csp3	Rotatable Bonds	H-bond Acceptors	H-bond Donors	MR	TPSA	Consensus Log P	ESOL Class	GI Absorption	BBB Permeant	Pgp Substrate	Lipinski Violations	Veber Violations	Bioavailability Score	PAINS Alerts	Brenk Alerts
9a	0.04	4	3	0	116.23	39.94	4.97	Poorly soluble	High	Yes	Yes	1	0	0.55	0	0
9b	0.08	4	3	0	121.19	39.94	5.29	Poorly soluble	High	No	Yes	1	0	0.55	0	0
9c	0.08	5	4	0	122.72	49.17	4.91	Poorly soluble	High	Yes	Yes	1	0	0.55	0	0
9d	0.04	4	4	0	116.19	39.94	5.27	Poorly soluble	High	No	Yes	1	0	0.55	0	0
9e	0.04	4	3	0	121.24	39.94	5.49	Poorly soluble	High	No	Yes	1	0	0.55	0	0
9f	0.04	4	3	0	123.93	39.94	5.57	Poorly soluble	High	No	Yes	1	0	0.55	0	0
9g	0.04	5	5	0	125.05	85.76	4.16	Poorly soluble	High	No	No	0	0	0.55	0	2
9h	0.11	6	5	0	129.21	58.4	4.92	Poorly soluble	High	No	Yes	0	0	0.55	0	0
14a	0.03	5	4	0	146.38	63.73	6.03	Poorly soluble	Low	No	No	1	0	0.55	0	0
14b	0.06	5	4	0	151.35	63.73	6.38	Poorly soluble	Low	No	No	1	0	0.55	0	0
14c	0.06	6	5	0	152.87	72.96	6	Poorly soluble	Low	No	No	2	0	0.17	0	0
14d	0.03	5	4	0	151.39	63.73	6.55	Poorly soluble	Low	No	No	2	0	0.17	0	0
14e	0.03	5	4	0	154.08	63.73	6.63	Poorly soluble	Low	No	No	2	0	0.17	0	0
14f	0.09	6	4	0	160.59	66.97	5.99	Poorly soluble	Low	No	No	2	0	0.17	0	0
14g	0.03	5	5	1	148.4	83.96	5.64	Poorly soluble	Low	No	No	1	0	0.55	0	0
14h	0.09	7	6	0	159.36	82.19	5.94	Poorly soluble	Low	No	No	1	0	0.55	0	0

Compounds **9g** and **9h** have zero violations of Lipinski's rule of five, whereas the rest have one violation, with the exception of **14c**–**f**, which has two violations. All compounds had acceptable clogP values in the range of 4.00–6.00. Topological polar surface area (TPSA) is the surface sum of all the polar atoms in a molecule, and the acceptable range is 20–130 Å, with all of our compounds falling inside this range. Except for **9a** and **9c**, none of the compounds penetrated the blood–brain barrier (BBB). Pgp is an efflux transporter that pushes xenobiotics out of cells, resulting in clearance [31,32]. Except for **9a**–**f** and **9h**, all compounds were anticipated to be non-substrates for P-gp. Except for **14c**–**f** compounds, all compounds had a bioavailability score of 0.55. Compounds **9a**–**h** have good GI absorption, whereas compounds **14a**–**h** have poor GI absorption. Except for **9g**, which has two brenk alerts, all compounds have zero pain and brenk alerts.

SwissADME provides a BOILED-Egg intrinsic model for predicting BBB entry and passive gastrointestinal absorption (HIA). It is a fantastic strategy that is based on two descriptors: WLOGP (lipophilicity) and TPSA (apparent polarity). The white region of the BOILED-Egg indicates a high likelihood of passive absorption through the gastrointestinal tract, but the yellow part indicates a high likelihood of reaching the brain. P-gp is a multidrug resistance efflux pump that is in charge of drug clearance. The presence or absence of PGP in a drug candidate is shown by blue or red spots in the BOILED-Egg plot.

Figure 12 illustrates the distribution of **9a**–**h** and **14a**–**h** on BOILED-Egg. Only **9a** and **9c** compounds were found in the yellow zone, indicating that they are BBB penetrant, whereas the remaining compounds are not. The presence of **9a**–**h** compounds in the white region indicated proper absorption, whereas **14a**–**h** compounds were identified outside the white region, indicating inadequate GI absorption. Among all compounds, seven were

anticipated to be P-gp substrates (PGP+) (blue dot), while the remaining compounds were not subjected to the active efflux P-gp pump (PGP-) (red dot).

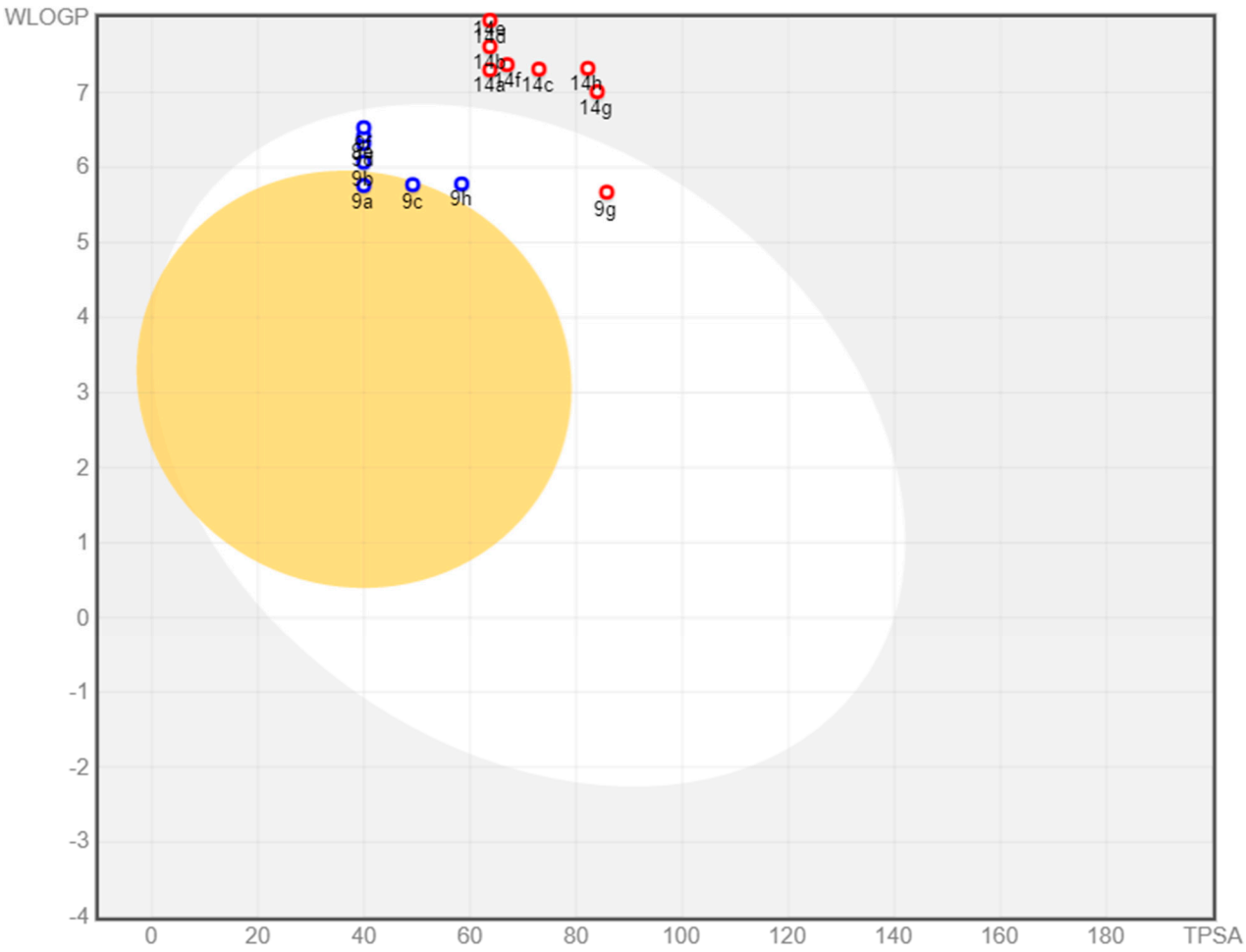

Figure 12. Spread of **9a**–**h** and **14a**–**h** compounds on the BOILED-Egg plot.

4. Conclusions

Novel two series pyrazolo[3,4-*b*]pyridine derivatives **9a**–**h** and **14a**–**h** were prepared and assessed for their anti-cancer activity against Hela, MCF7, and HCT-116 cancer cell lines. Compounds **9a** and **14g** showed the highest anticancer activity, the highest cell cycle arrest, and a significant level of early and late apoptosis. They showed good safety profiles on normal cell line WI-38. They also showed good inhibition activity towards CDK2 and CDK9. Compounds **9a** and **14g** showed essential interactions in their docking in CDK2 and CDK9 active sites. In the light of these results, the situation definitely calls for additional research to understand the effect of substitutions around pyrazolo[3,4-*b*]pyridine central moiety and the activity of a such class of compounds.

5. Experimental Section

5.1. Chemistry

2-Bromo-1-(phenyl/4-methoxyphenyl)ethan-1-ones **2a**, **b** [33], 3-(phenyl/4-methoxyphenyl)-3-oxopropanenitriles **3a**, **b** [34], aminopyrazole **4b** [35], and enamenones **5a**–**g** [36] were prepared following the reported method. Instruments and thermal analysis results are listed in Supporting Data.

5.1.1. Synthesis of Pyrazolo[3,4-*b*]pyridine Derivatives **9a**–**h**

A mixture of 3-(4-methoxyphenyl)-1-phenyl-1*H*-pyrazol-5-amine (**4b**) (0.265 g, 1 mmol) and enamenones **6a**–**h** (1 mmol) in glacial acetic acid (30 mL) was refluxed for 4–6 h. After cooling, the formed precipitate was filtered, washed with EtOH, and crystallized from EtOH/DMF to yield the corresponding pyrazolo[3,4-*b*]pyridine derivatives **9a**–**h**, respectively.

3-(4-Methoxyphenyl)-1,4-diphenyl-1*H*-pyrazolo[3,4-*b*]pyridine (**9a**)

White powder, 72% yield; mp 161–163 °C; IR ν_{max}/cm^{-1} 1593 (C=N), 1501 (C=C), 1250 (C–O); ^{1}H-NMR δ 3.87 (s, 3H, OMe), 7.16 (d, *J* = 8.8 Hz, 2H, ArHs), 7.39 (t, *J* = 7.4 Hz, 1H, ArH), 7.51–7.67 (m, 5H, ArHs), 8.01 (d, *J* = 8.5 Hz, 1H, H3 of pyridine), 8.09 (d, *J* = 8.7 Hz, 2H, ArHs), 8.27 (d, *J* = 7.3 Hz, 2H, ArHs), 8.46 (d, *J* = 7.2 Hz, 2H, ArHs), 8.70 (d, *J* = 8.5 Hz, 1H, H2 of pyridine); ^{13}C-NMR δ 55.77 (C of OMe), 113.95, 115.03 (2C), 115.99, 121.05 (2C), 125.01, 126.23, 127.80 (2C), 128.85 (2C), 129.48 (2C), 129.70 (2C), 130.33, 132.65, 138.62, 139.68, 143.92, 151.39, 156.42, 160.38; MS *m/z* (%) 377.08 (M^+,21.80). For $C_{25}H_{19}N_3O$ (377.45): Calc.: C, 79.55; H, 5.07; N, 11.13. Found: C, 79.31; H, 5.20; N, 11.40.

3-(4-Methoxyphenyl)-1-phenyl-4-(p-tolyl)-1*H*-pyrazolo[3,4-*b*]pyridine (**9b**)

White powder, 75% yield; mp 186–188 °C; IR ν_{max}/cm^{-1} 1593 (C=N), 1501 (C=C), 1250 (C–O); ^{1}H-NMR δ 2.41 (s, 3H, Me), 3.87 (s, 3H, OMe), 7.16 (d, *J* = 8.8 Hz, 2H, ArHs), 7.39 (d, *J* = 8.0 Hz, 3H, ArHs), 7.64 (t, *J* = 7.8 Hz, 2H, ArHs), 7.99 (d, *J* = 8.6 Hz, 1H, H3 of pyridine), 8.09 (d, *J* = 8.9 Hz, 2H, ArHs), 8.17 (d, *J* = 8.4 Hz, 2H, ArHs), 8.46 (d, *J* = 8.6 Hz, 2H, ArHs), 8.69 (d, *J* = 8.5 Hz, 1H, H2 of pyridine); ^{13}C-NMR δ 21.38 (C of Me), 55.75 (C of OMe), 113.73, 115.01 (2C), 115.70, 120.99 (2C), 125.05, 126.17, 127.68 (2C), 128.82 (2C), 129.68 (2C), 130.07 (2C), 132.50, 135.84, 139.72, 140.07, 143.88, 151.40, 156.42, 160.35; MS *m/z* (%) 391.47 (M^+, 52.80). For $C_{26}H_{21}N_3O$ (391.47): Calc.: C, 79.77; H, 5.41; N, 10.73. Found: C, 79.54; H, 5.68; N, 10.98.

3,4-Bis(4-methoxyphenyl)-1-phenyl-1*H*-pyrazolo[3,4-*b*]pyridine (**9c**)

White powder, 66% yield; mp 198–200 °C; IR ν_{max}/cm^{-1} 1600 (C=N), 1501(C=C), 1254 (C–O); ^{1}H-NMR δ 3.855 (s, 3H, OMe), 3.865 (s, 3H, OMe), 7.09–7.18 (m, 4H, ArHs), 7.37 (t, *J* = 7.4 Hz, 1H, ArH), 7.63 (t, *J* = 7.8 Hz, 2H, ArHs), 7.94 (d, *J* = 8.6 Hz, 1H, H3 of pyridine), 8.07 (d, *J* = 8.6 Hz, 2H, ArHs), 8.23 (d, *J* = 8.7 Hz, 2H, ArHs), 8.45 (d, *J* = 8.0 Hz, 2H, ArHs), 8.63 (d, *J* = 8.5 Hz, 1H, H2 of pyridine); ^{13}C-NMR δ 55.75 (C of OMe), 55.79 (C of OMe), 113.38, 114.86 (2C), 115.01 (2C), 115.34, 120.96 (2C), 125.09, 126.13, 128.81 (2C), 129.24 (2C), 129.67 (2C), 130.98, 132.42, 139.75, 143.88, 151.44, 156.20, 160.33, 161.29; MS *m/z* (%) 407.33 (M^+, 14.18). For $C_{26}H_{21}N_3O_2$ (407.47): Calc.: C, 76.64; H, 5.19; N, 10.31. Found: C, 76.86; H, 5.32; N, 10.47.

4-(4-Fluorophenyl)-3-(4-methoxyphenyl)-1-phenyl-1*H*-pyrazolo[3,4-*b*]pyridine (**9d**)

White powder, 74% yield; mp 171–173 °C; IR ν_{max}/cm^{-1} 1597 (C=N), 1505 (C=C), 1250 (C–O), 1227 (C-F); ^{1}H-NMR δ 3.87 (s, 3H, OMe), 7.15 (d, *J* = 8.7 Hz, 2H, ArHs), 7.40 (q, *J* = 8.6 Hz, 3H, ArHs), 7.63 (t, *J* = 7.9 Hz, 2H, ArHs), 8.00 (d, *J* = 8.5 Hz, 1H, H3 of pyridine), 8.08 (d, *J* = 8.7 Hz, 2H, ArHs), 8.33 (dd, *J* = 8.7, 5.7 Hz, 2H, ArHs), 8.43 (d, *J* = 8.6 Hz, 2H, ArHs), 8.70 (d, *J* = 8.5 Hz, 1H, H2 of pyridine); ^{13}C-NMR δ 55.77 (C of OMe), 113.86, 115.03 (2C), 115.82, 116.27, 116.49, 121.11 (2C), 124.96, 126.28, 128.86 (2C), 129.71 (2C), 130.02, 130.11, 132.77, 134.76, 139.62, 143.93, 151.28, 155.36, 160.39, 165.03; MS *m/z* (%) 395.64 (M^+, 26.35). For $C_{25}H_{18}FN_3O$ (395.44): Calc.: C, 75.93; H, 4.59; N, 10.63. Found: C, 76.09; H, 4.72; N, 10.91.

4-(4-Chlorophenyl)-3-(4-methoxyphenyl)-1-phenyl-1*H*-pyrazolo[3,4-*b*]pyridine (**9e**)

White powder, 72% yield; mp 210–212 °C; IR ν_{max}/cm^{-1} 1599 (C=N), 1501 (C=C), 1254 (C–O); ^{1}H-NMR δ 3.87 (s, 3H, OMe), 7.15 (d, *J* = 8.4 Hz, 2H, ArHs), 7.39 (t, *J* = 7.4 Hz, 1H, ArH), 7.63 (dd, *J* = 8.3, 6.3 Hz,, 4H, ArHs), 8.03 (d, *J* = 8.5 Hz, 1H, H3 of pyridine), 8.09 (d,

J = 8.6 Hz, 2H, ArHs), 8.29 (d, *J* = 8.3 Hz, 2H, ArHs), 8.42 (d, *J* = 8.0 Hz, 2H, ArHs), 8.72 (d, *J* = 8.6 Hz, 1H, H2 of pyridine); ^{13}C-NMR δ 55.78 (C of OMe), 110.10, 115.08, 115.96, 121.18 (2C), 122.66, 124.92, 126.63, 128.89, 129.56 (2C), 129.75 (2C), 135.61, 137.43, 139.56, 144.00, 149.39, 151.27, 152.74, 153.76, 155.17, 160.42, 161.98; MS *m/z* (%) 412.40 (M^++1, 36.04), 411.71 (M^+, 53.37). For $C_{25}H_{18}ClN3O$ (411.89): Calc.: C, 72.90; H, 4.41; N, 10.20. Found: C, 73.14; H, 4.60; N, 10.43.

4-(4-Bromophenyl)-3-(4-methoxyphenyl)-1-phenyl-1*H*-pyrazolo[3,4-*b*]pyridine (**9f**)

Pale yellow powder, 65% yield; mp 217–219 °C; IR ν_{max}/cm^{-1} 1596 (C=N), 1501 (C=C), 1254 (C–O), 1227 (C–F); ^{1}H-NMR δ 3.86 (s, 3H, OMe), 7.14 (d, *J* = 8.2 Hz, 2H, ArHs), 7.38 (t, *J* = 7.4 Hz, 1H, ArHs), 7.62 (t, *J* = 7.8 Hz, 2H, ArHs), 7.76 (d, *J* = 8.1 Hz, 2H, ArHs), 7.99 (d, *J* = 8.5 Hz, 1H, H3 of pyridine), 8.07 (d, *J* = 8.2 Hz, 2H, ArHs), 8.19 (d, *J* = 8.1 Hz, 2H, ArHs), 8.41 (d, *J* = 8.0 Hz, 2H, ArHs), 8.69 (d, *J* = 8.5 Hz, 1H, H2 of pyridine); ^{13}C-NMR δ 55.76 (C of OMe), 107.26, 114.15, 115.23 (2C), 115.92, 121.15 (2C), 126.47, 128.85, 129.65, 129.76 (2C), 131.76 (2C), 132.13, 143.93, 139.75, 145.47, 151.24, 154.43, 154.97, 157.59, 162.42, 166.54; MS *m/z* (%) 456.20 (M^+, 23.09). For $C_{25}H_{18}BrN_3O$ (456.34): Calc.: C, 65.80; H, 3.98; N, 9.21. Found: C, 65.97; H, 4.06; N, 9.42.

3-(4-Methoxyphenyl)-4-(4-nitrophenyl)-1-phenyl-1*H*-pyrazolo[3,4-*b*]pyridine (**9g**)

Orange powder, 68% yield; mp > 300 °C; IR ν_{max}/cm^{-1} 1597 (C=N), 1520 (C-NO_2), 1497 (C=C), 1343 (C–NO_2), 1250 (C–O); ^{1}H-NMR δ 3.88 (s, 3H, OMe), 7.18 (d, *J* = 8.3 Hz, 2H, ArHs), 7.42 (s, 1H, ArH), 7.67 (d, *J* = 8.2 Hz, 3H, ArHs), 8.16–8.43 (m, 7H, 6 ArHs + H3 of pyridine), (d, *J* = 8.1 Hz, 4H, ArHs), 8.56 (d, *J* = 8.4 Hz, 2H, H2 of pyridine); MS *m/z* (%) 422.27 (M^+, 43.75). For $C_{25}H_{18}NO_3$ (422.44): Calc.: C, 71.08; H, 4.30; N, 13.26. Found: C, 70.89; H, 4.57; N, 13.47.

4-(3,4-Dimethoxyphenyl)-3-(4-methoxyphenyl)-1-phenyl-1*H*-pyrazolo[3,4-*b*]pyridine (**9h**)

White powder, 76% yield; mp 165–167 °C; IR ν_{max}/cm^{-1} 1593 (C=N), 1520, 1505 (C=C), 1250 (C–O–C); ^{1}H-NMR δ 3.86 (s, 3H, OMe), 3.87 (s, 3H, OMe), 3.93 (s, 3H, OMe), 7.14 (dd, *J* = 8.5, 6.0 Hz, 3H, ArHs), 7.37 (t, *J* = 7.4 Hz, 1H, ArHs), 7.59–7.67 (m, 2H, ArHs), 7.82–7.91 (m, 2H, ArHs), 8.00 (d, *J* = 8.6 Hz, 1H, H3 of pyridine), 8.08 (d, *J* = 8.8 Hz, 2H, ArHs), 8.48 (d, *J* = 7.4 Hz, 2H, ArHs), 8.63 (d, *J* = 8.6 Hz, 1H, H2 of pyridine); ^{13}C-NMR δ 55.74 (C of OMe), 55.90 (C of OMe), 56.07 (C of OMe), 110.77, 112.28, 115.01, 115.44 (2C), 120.72, 120.90 (2C), 125.07, 126.14, 128.80 (2C), 129.63 (2C), 131.06, 132.30, 139.69, 143.89, 149.43, 151.02, 151.32, 156.12, 160.32; MS *m/z* (%) 437.66 (M^+, 21.67). For $C_{27}H_{23}N_3O_3$ (437.50): Calc.: C, 74.13; H, 5.30; N, 9.60. Found: C, 74.40; H, 5.42; N, 9.78.

5.1.2. Synthesis of Pyrazolo[3,4-*b*]pyridine Derivatives **14a**–**g**

A mixture of aminopyrazole **4b** (0.265 g, 1 mmol), propanenitrile **3a** (0.145 g, 1 mmol), and the appropriate aromatic aldehydes **10a**–**g** (1 mmol) in absolute EtOH (30 mL) was refluxed for 6–10 h in the presence of TEA (catalytic). The formed precipitated was filtered, washed with EtOH, and crystallized from EtOH/DMF to yield pyrazolo[3,4-*b*]pyridine derivatives **14a**–**h**, respectively.

3-(4-Methoxyphenyl)-1,4,6-triphenyl-1*H*-pyrazolo[3,4-*b*]pyridine-5-carbonitrile (**14a**)

White powder, 74% yield; mp 229–231 °C; IR ν_{max}/cm^{-1} 2218 (C≡N), 1610 (C=N), 1559, 1497 (C=C), 1250 (C–O); ^{1}H-NMR δ 3.72 (s, 3H, OMe), 6.65 (d, *J* = 8.7 Hz, 2H, ArHs), 7.03 (d, *J* = 8.6 Hz, 2H), 7.32 (t, *J* = 7.5 Hz, 2H, ArHs), 7.39–7.47 (m, 4H, ArHs), 7.60–7.66 (m, 5H, ArHs), 8.00–8.02 (m, 2H, ArHs), 8.29 (d, *J* = 7.4 Hz, 2H); ^{13}C-NMR δ 55.61 (C of OMe), 102.37, 112.26, 113.54 (2C), 118.02, 122.04 (2C), 123.87, 127.35, 128.50 (2C), 128.99 (2C), 129.78 (2C), 129.85 (2C), 129.94 (2C), 130.07, 130.54 (2C), 130.70, 133.93, 138.10, 138.66, 147.06, 150.28, 153.02, 159.66, 160.76; MS *m/z* (%) 478.58 (M^+, 15.55). For $C_{32}H_{22}N_4O$ (478.56): Calc.: C, 80.32; H, 4.63; N, 11.71. Found: C, 80.09; H, 4.74; N, 11.94.

3-(4-Methoxyphenyl)-1,6-diphenyl-4-(p-tolyl)-1*H*-pyrazolo[3,4-*b*]pyridine-5-carbonitrile (**14b**)

White powder, 68% yield; mp 203–205 °C; IR ν_{max}/cm^{-1} 2218 (C≡N), 1609, (C=N), 1559, 1509 (C=C), 1250 (C–O); ^{1}H-NMR δ 2.34 (s, 3H, Me), 3.72 (s, 3H, OMe), 6.64 (d, *J* = 8.7 Hz, 2H, ArHs), 7.00 (d, *J* = 8.7 Hz, 2H, ArHs), 7.10 (d, *J* = 7.9 Hz, 2H, ArHs), 7.25 (d, *J* = 8.1 Hz, 2H, ArHs), 7.42 (t, *J* = 7.5 Hz, 1H, ArHs), 7.57–7.65 (m, 5H, ArHs), 7.99–8.01 (m, 2H, ArHs), 8.28 (d, *J* = 8.5 Hz, 2H, ArHs); ^{13}C-NMR δ 21.32 (C of Me), 55.64 (C of OMe), 102.28, 112.39, 113.46 (2C), 118.11, 122.05 (2C), 123.91, 127.34, 128.97 (2C), 129.79 (2C), 129.92 (2C), 130.58 (2C), 130.67, 131.04, 138.13, 138.67, 139.85, 147.10, 150.27, 153.19, 159.70, 160.79; MS *m/z* (%) 492.77 (M^+, 58.66). For $C_{33}H_{24}N_4O$ (492.58): Calc.: C, 80.47; H, 4.91; N, 11.37. Found: C, 80.68; H, 4.85; N, 11.53.

3,4-Bis(4-methoxyphenyl)-1,6-diphenyl-1*H*-pyrazolo[3,4-*b*]pyridine-5-carbonitrile (**14c**)

White powder, 65% yield; mp 207–209 °C; IR ν_{max}/cm^{-1} 2218 (C≡N), 1609 (C=N), 1551, 1509 (C=C), 1250 (C–O); ^{1}H-NMR δ 3.74 (s, 3H, OMe), 3.78 (s, 3H, OMe), 6.69 (d, *J* = 8.7 Hz, 2H, ArHs), 6.84 (d, *J* = 8.7 Hz, 2H, ArHs), 7.04 (d, *J* = 8.7 Hz, 2H, ArHs), 7.31 (d, *J* = 8.6 Hz, 2H, ArHs), 7.43 (t, *J* = 7.4 Hz, 1H, ArHs), 7.58–7.68 (m, 5H, ArHs), 7.99 - 8.02 (m, 2H, ArHs), 8.29 (d, *J* = 8.5 Hz, 2H, ArHs); ^{13}C-NMR δ 55.66 (C of OMe), 55.83 (C of OMe), 102.36, 112.51, 113.58 (2C), 113.97 (2C), 118.26, 122.09 (2C), 124.06, 125.96, 127.35, 128.98 (2C), 129.82 (2C), 129.95 (2C), 130.66 (3C), 131.56 (2C), 138.23, 138.73, 147.22, 150.33, 152.99, 159.70, 160.87, 160.94; MS *m/z* (%) 508.37 (M^+, 24.90). For $C_{33}H_{24}N_4O_2$ (508.58): Calc.: C, 77.94; H, 4.76; N, 11.02. Found: C, 78.12; H, 4.92; N, 11.24.

4-(4-Chlorophenyl)-3-(4-methoxyphenyl)-1,6-diphenyl-1*H*-pyrazolo[3,4-*b*]pyridine-5-carbonitrile (**14d**)

White powder, 70% yield; mp 258–260 °C; IR ν_{max}/cm^{-1} 2226 (C≡N), 1610 (C=N), 1493 (C=C), 1250 (C–O); ^{1}H-NMR δ 3.74 (s, 3H, OMe), 6.69 (d, *J* = 6.5 Hz, 2H, ArHs), 7.02 (d, *J* = 6.4 Hz, 2H, ArHs), 7.45–7.32 (m, 5H, ArHs) 7.59–7.63 (m, 5H, ArHs), 8.01 (d, *J* = 6.7, Hz, 2H, ArHs), 8.28 (d, *J* = 8.2 Hz, 2H, ArHs); ^{13}C-NMR δ 55.71 (C of OMe), 112.77, 113.61 (2C), 115.61, 117.88, 122.07 (2C), 123.73, 127.44, 128.48 (2C), 129.04 (3C), 129.85 (3C), 129.93 (2C), 130.72 (2C), 130.77 (2C), 131.75 (2C), 132.69, 135.16, 138.04, 138.65, 150.23, 159.87; MS *m/z* (%) 514.87, (M^++1, 19.95), 513.02 (M^+, 46.40). For $C_{32}H_{21}ClN_4O$ (513.00): Calc.: C, 74.92; H, 4.13; N, 10.92. Found: C, 74.81; H, 4.29; N, 11.15.

4-(4-Bromophenyl)-3-(4-methoxyphenyl)-1,6-diphenyl-1*H*-pyrazolo[3,4-*b*]pyridine-5-carbonitrile (**14e**)

White powder, 82% yield; mp 221–223 °C; IR ν_{max}/cm^{-1} 2226 (C≡N), 1609 (C=N), 1524, 1489 (C=C), 1250 (C-O); ^{1}H-NMR δ 3.76 (s, 3H, OMe), 6.70 (d, *J* = 8.7 Hz, 2H, ArHs), 7.02 (d, *J* = 8.7 Hz, 2H, ArHs), 7.32 (d, *J* = 8.4 Hz, 2H, ArHs), 7.42 (t, *J* = 7.4 Hz, 1H, ArHs), 7.50 (d, *J* = 8.5 Hz, 2H, ArHs), 7.58–7.69 (m, 5H, ArHs), 8.00–8.02 (m, 2H, ArHs), 8.29 (d, *J* = 7.3 Hz, 2H, ArHs); ^{13}C-NMR δ 55.68 (C of OMe), 102.07, 112.40, 113.55 (2C), 117.87, 121.93 (2C), 123.63, 123.85, 127.37, 129.03 (2C), 129.80 (2C), 129.90 (2C), 130.67 (2C), 130.78, 131.38 (2C), 131.90 (2C), 132.97, 137.96, 138.60, 146.98, 150.18, 151.70, 159.81, 160.70; MS *m/z* (%) 559.62 (M^++2, 7.68), 557.96 (M^+, 25.99). For $C_{32}H_{21}BrN_4O$ (557.45): Calc.: C, 68.95; H, 3.80; N, 10.05. Found: C, 69.07; H, 3.94; N, 10.21.

4-(4-(Dimethylamino)phenyl)-3-(4-methoxyphenyl)-1,6-diphenyl-1*H*-pyrazolo[3,4-*b*]pyridine-5-carbonitrile (**14f**)

Pale yellow powder, 63% yield; mp 230–232 °C; IR ν_{max}/cm^{-1} 2218 (C≡N), 1613 (C=N), 1524, 1489 (C=C), 1250 (C–O); ^{1}H-NMR δ 2.93 (s, 6H, 2NMe), 3.74 (s, 3H, OMe), 6.55 (d, *J* = 8.9 Hz, 2H, ArHs), 6.68 (d, *J* = 8.8 Hz, 2H, ArHs), 7.05 (d, *J* = 8.7 Hz, 2H, ArHs), 7.17 (d, *J* = 8.8 Hz, 2H, ArHs), 7.42 (t, *J* = 7.5 Hz, 1H, ArHs), 7.57–7.66 (m, 5H, ArHs), 7.98–8.01

(m, 2H, ArHs), 8.29 (d, *J* = 7.3 Hz, 2H); ^{13}C-NMR δ 40.31 (2C of 2Me), 55.60 (C of OMe), 101.81, 111.59 (2C), 112.28, 113.57 (2C), 118.69, 120.52, 122.08, 124.36, 127.26, 128.92 (2C), 129.78 (2C), 129.95 (2C), 130.54, 130.67 (2C), 131.22 (2C), 138.42, 138.81, 147.39, 150.45, 151.75, 153.68, 159.56, 161.08; MS *m/z* (%) 521.28 (M^+, 19.10). For $C_{34}H_{27}N_5O$ (521.62): Calc.: C, 78.29; H, 5.22; N, 13.43. Found: C, 78.43; H, 5.46; N, 13.67.

4-(4-Hydroxyphenyl)-3-(4-methoxyphenyl)-1,6-diphenyl-1*H*-pyrazolo[3,4-*b*]pyridine-5-carbonitrile (**14g**)

White powder, 77% yield; mp 295–297 °C; IR ν_{max}/cm^{-1} 2222 (C≡N), 1613 (C=N), 1555, 1512 (C=C), 1250 (C–O); ^{1}H-NMR δ 3.74 (s, 3H, OMe), 6.68 (dd, *J* = 13.4, 8.7 Hz, 4H, ArHs), 7.06 (d, *J* = 8.7 Hz, 2H, ArHs), 7.18 (d, *J* = 8.6 Hz, 2H, ArHs), 7.41 (t, *J* = 7.4 Hz, 1H, ArH), 7.63–7.57 (m, 5H, ArHs), 8.02–7.97 (m, 2H, ArHs), 8.28 (dd, *J* = 8.7, 1.2 Hz, 2H, ArHs), 9.90 (s, D_2O exchangeable, 1H, OH); ^{13}C-NMR δ 55.68 (C of OMe), 102.30, 112.32, 113.57 (2C), 115.25 (2C), 118.38, 122.05, 124.19, 124.34, 127.28, 128.94 (2C), 129.77 (2C), 129.94 (2C), 130.60, 130.71 (2C), 131.65 (2C), 138.28, 138.75, 147.23, 150.39, 153.39, 159.44, 159.70, 160.92; MS *m/z* (%) 494.63 (M^+, 13.48). For $C_{32}H_{22}N_4O_2$ (494.55): Calc.: C, 77.72; H, 4.48; N, 11.33. Found: C, 77.50; H, 4.52; N, 11.50.

4-(3,4-Dimethoxyphenyl)-3-(4-methoxyphenyl)-1,6-diphenyl-1*H*-pyrazolo[3,4-*b*]pyridine-5-carbonitrile (**14h**)

White powder, 69% yield; mp 212–214 °C; IR ν_{max}/cm^{-1} 2222 (C≡N), 1609 (C=N), 1555, 1505 (C=C), 1258 (C–O); ^{1}H-NMR δ 3.37 (s, 3H, OMe), 3.73 (s, 3H, OMe), 3.82 (s, 3H, OMe), 6.70 (d, *J* = 8.4 Hz, 2H, ArHs), 6.77 (d, *J* = 2.1 Hz, 1H, ArHs), 7.03 (dd, *J* = 14.1, 8.3 Hz, 3H, ArHs), 7.15 (dd, *J* = 8.2, 2.0 Hz, 1H, ArHs), 7.42 (t, *J* = 7.4 Hz, 1H, ArHs), 7.58–7.66 (m, 5H, ArHs), 7.99–8.02 (m, 2H, ArHs), 8.28 (d, *J* = 8.0 Hz, 2H, ArHs); ^{13}C-NMR δ 55.60 (C of OMe), 55.73 (C of OMe), 56.22 (C of OMe), 102.24, 111.90, 112.33, 113.52 (2C), 114.48, 118.36, 122.13 (2C), 122.83, 124.36, 126.01, 127.36, 128.97 (2C), 129.81 (2C), 129.95 (2C), 130.64, 130.68 (2C), 138.25, 138.72, 147.18, 148.68, 150.35, 150.68, 152.93, 159.78, 160.94; MS *m/z* (%) 538.16 (M^+, 27.45). For $C_{34}H_{26}N_4O_3$ (538.61): Calc.: C, 75.82; H, 4.87; N, 10.40. Found: C, 75.96; H, 4.98; N, 10.68.

5.2. Biological Screening

5.2.1. MTT Assay for Cytotoxicity

Standard MTT colorimetric assay was applied to test the IC_{50} of compounds **9a**–**h** and **14a**–**h** against three cell lines, namely, cervical cancer Hela, breast cancer MCF7, and colon HCT-116, compared with doxorubicin as a reference compound with the typical reported methodology of MTT colorimetric assay [37].

5.2.2. Cell Cycle Analysis and Apoptotic Assay

Cell cycle analysis and apoptosis study of the 2 most active compounds, **9a** and **14g**, was accomplished using propidium iodide (PI) flow cytomertric analysis according to the reported procedure [38,39]. An apoptotic study using the Annexin V-FITC Apoptosis Detection Kit (K101–25, BioVision®, 980 Linda Vista Avenue, Mountain View, CA, USA) at their IC_{50} concentration values was used on the specified cell after 24 h in three successive steps according to the manufacturer's instructions.

5.2.3. In Vitro CDK Enzyme Assay

The CDK in vitro inhibitory activity of **9a**–**h** and **14a**–**h** toward CDK2 and CDK9 was performed using CDK Assay Kit (BPS Bioscience, USA) at different dilutions of 30, 10, 3, 1, 0.3, 0.1, 0.03, and 0.01 µM, measuring the chemiluminescence using BioTek™ Synergy2 Microplate Reader (BioTek, Santa Clara, CA, USA) [40].

5.3. Molecular Docking

Docking studies of compounds **9a** and **14g** were performed using Molecular Operating Environment (MOE 2019.02) software [41–43], and the crystal structures of CDK2 and CDK9 in complex with CAN508 were downloaded from the protein databank PDB IDs 3tnw and 3tn8, respectively.

5.4. In-Silico SwissADME Predictions

SwissADME is a reliable, free online utility [44] for calculating the physicochemical properties of compounds. By uploading the structures to the website http://www.swissadme.ch/, accessed on 10 March 2023, the bioavailability and pharmacokinetic parameters of any synthetic compound can be determined. The smiles of **9a**–**9h** and **14a**–**14h** structures were imported into the SwissADME environment. Different physiological and pharmacokinetic parameter measurements were exported as a CSV file, from which data were extracted and analyzed.

Supplementary Materials: The following supporting information can be downloaded at: https://www.mdpi.com/article/10.3390/molecules28176428/s1, Figure S1−S64: NMR spectra; Figure S65−S80: IR spectra; Figure S81−S94: Mass spectra.

Author Contributions: Conceptualization, methodology, software, validation, formal analysis, F.A.B., A.A.-M.A.-A. and S.T.A.-R.; investigation, B.S.A.; resources, data curation, writing—original draft preparation, writing—review and editing, visualization, B.S.A., F.A.B., A.A.-M.A.-A. and S.T.A.-R.; supervision, project administration, F.A.B., A.A.-M.A.-A. and S.T.A.-R.; funding acquisition, S.T.A.-R. All authors have read and agreed to the published version of the manuscript.

Funding: This research was funded by National Institute for Health Research, grant number SNIH-RO-HRT01-2302-KSU-36598045, Riyadh, Saudi Arabia.

Institutional Review Board Statement: Not applicable.

Informed Consent Statement: Not applicable.

Data Availability Statement: Not applicable.

Acknowledgments: The authors acknowledge the support from National Institute for Health Research under project No. SNIH-RO-HRT01-2302-KSU-36598045, Riyadh, Saudi Arabia.

Conflicts of Interest: The authors declare no conflict of interest.

Sample Availability: Samples of the compounds are not available from the authors.

References

1. Hanahan, D.; Weinberg, R.A. Hallmarks of Cancer: The Next Generation. *Cell* **2011**, *144*, 646–674. [CrossRef]
2. Balter, M.; Vogel, G. Cycling toward Stockholm. *Science* **2001**, *294*, 502–503. [CrossRef]
3. Roskoski, R., Jr. Cyclin-dependent protein kinase inhibitors including palbociclib as anticancer drugs. *Pharmacol. Res.* **2016**, *107*, 249–275. [CrossRef]
4. Malumbres, M.; Barbacid, M. Mammalian cyclin-dependent kinases. *Trends Biochem. Sci.* **2005**, *30*, 630–641. [CrossRef]
5. Yin, T.; Lallena, M.J.; Kreklau, E.L.; Fales, K.R.; Carballares, S.; Torrres, R.; Wishart, G.N.; Ajamie, R.T.; Cronier, D.M.; Iversen, P.W. A novel CDK9 inhibitor shows potent antitumor efficacy in preclinical hematologic tumor models. *Mol. Cancer Ther.* **2014**, *13*, 1442–1456. [CrossRef]
6. Jessen, B.A.; Lee, L.; Koudriakova, T.; Haines, M.; Lundgren, K.; Price, S.; Nonomiya, J.; Lewis, C.; Stevens, G.J. Peripheral white blood cell toxicity induced by broad spectrum cyclin-dependent kinase inhibitors. *J. Appl. Toxicol. Int. J.* **2007**, *27*, 133–142. [CrossRef]
7. Abate, A.A.; Pentimalli, F.; Esposito, L.; Giordano, A. ATP-noncompetitive CDK inhibitors for cancer therapy: An overview. *Exp. Opin. Investig. Drugs* **2013**, *22*, 895–906. [CrossRef]
8. Sanchez-Martinez, C.; Gelbert, L.M.; Lallena, M.J.; de Dios, A. Cyclin dependent kinase (CDK) inhibitors as anticancer drugs. *Bioorg. Med. Chem. Lett.* **2015**, *25*, 3420–3435. [CrossRef]
9. Awan, F.T.; Jones, J.A.; Maddocks, K.; Poi, M.; Grever, M.R.; Johnson, A.; Byrd, J.C.; Andritsos, L.A. A phase 1 clinical trial of flavopiridol consolidation in chronic lymphocytic leukemia patients following chemoimmunotherapy. *Ann. Hematol.* **2016**, *95*, 1137–1143. [CrossRef]

10. Zeidner, J.F.; Foster, M.C.; Blackford, A.L.; Litzow, M.R.; Morris, L.E.; Strickland, S.A.; Lancet, J.E.; Bose, P.; Levy, M.Y.; Tibes, R. Randomized multicenter phase II study of flavopiridol (alvocidib), cytarabine, and mitoxantrone (FLAM) versus cytarabine/daunorubicin (7+3) in newly diagnosed acute myeloid leukemia. *Haematologica* **2015**, *100*, 1172. [CrossRef]
11. Cicenas, J.; Kalyan, K.; Sorokinas, A.; Stankunas, E.; Levy, J.; Meskinyte, I.; Stankevicius, V.; Kaupinis, A.; Valius, M. Roscovitine in cancer and other diseases. *Ann. Trans. Med.* **2015**, *3*, 135.
12. Meijer, L.; Borgne, A.; Mulner, O.; Chong, J.P.; Blow, J.J.; Inagaki, N.; Inagaki, M.; Delcros, J.G.; Moulinoux, J.P. Biochemical and cellular effects of roscovitine, a potent and selective inhibitor of the cyclin-dependent kinases cdc2, cdk2 and cdk5. *Eur. J. Biochem.* **1997**, *243*, 527–536. [CrossRef]
13. Saqub, H.; Proetsch-Gugerbauer, H.; Bezrookove, V.; Nosrati, M.; Vaquero, E.M.; de Semir, D.; Ice, R.J.; McAllister, S.; Soroceanu, L.; Kashani-Sabet, M.; et al. Dinaciclib, a cyclin-dependent kinase inhibitor, suppresses cholangiocarcinoma growth by targeting CDK2/5/9. *Sci. Rep.* **2020**, *10*, 18489. [CrossRef]
14. Paruch, K.; Dwyer, M.P.; Alvarez, C.; Brown, C.; Chan, T.Y.; Doll, R.J.; Keertikar, K.; Knutson, C.; McKittrick, B.; Rivera, J.; et al. Discovery of Dinaciclib (SCH 727965): A Potent and Selective Inhibitor of Cyclin-Dependent Kinases. *ACS Med. Chem. Lett.* **2010**, *1*, 204–208. [CrossRef]
15. Bennani, F.E.; Doudach, L.; Cherrah, Y.; Ramli, Y.; Karrouchi, K.; Ansar, M.; Faouzi, M.E.A. Overview of recent developments of pyrazole derivatives as an anticancer agent in different cell line. *Bioorg. Chem.* **2020**, *97*, 103470. [CrossRef]
16. Palomer, A.; Cabré, F.; Pascual, J.; Campos, J.; Trujillo, M.A.; Entrena, A.; Gallo, M.A.; García, L.; Mauleón, D.; Espinosa, A. Identification of novel cyclooxygenase-2 selective inhibitors using pharmacophore models. *J. Med. Chem.* **2002**, *45*, 1402–1411. [CrossRef]
17. Kulp, S.K.; Yang, Y.-T.; Hung, C.-C.; Chen, K.-F.; Lai, J.-P.; Tseng, P.-H.; Fowble, J.W.; Ward, P.J.; Chen, C.-S. 3-phosphoinositide-dependent protein kinase-1/Akt signaling represents a major cyclooxygenase-2-independent target for celecoxib in prostate cancer cells. *Cancer Res.* **2004**, *64*, 1444–1451. [CrossRef]
18. Staben, S.T.; Heffron, T.P.; Sutherlin, D.P.; Bhat, S.R.; Castanedo, G.M.; Chuckowree, I.S.; Dotson, J.; Folkes, A.J.; Friedman, L.S.; Lee, L. Structure-based optimization of pyrazolo-pyrimidine and-pyridine inhibitors of PI3-kinase. *Bioorg. Med. Chem. Lett.* **2010**, *20*, 6048–6051. [CrossRef]
19. Chiacchio, M.A.; Iannazzo, D.; Romeo, R.; Giofrè, S.V.; Legnani, L. Pyridine and pyrimidine derivatives as privileged scaffolds in biologically active agents. *Curr. Med. Chem.* **2019**, *26*, 7166–7195. [CrossRef]
20. Tadesse, S.; Caldon, E.C.; Tilley, W.; Wang, S. Cyclin-Dependent Kinase 2 Inhibitors in Cancer Therapy: An Update. *J. Med. Chem.* **2019**, *62*, 4233–4251. [CrossRef]
21. Donaire-Arias, A.; Montagut, A.M.; de la Bellacasa, R.P.; Estrada-Tejedor, R.; Teixidó, J.; Borrell, J.I. 1H-Pyrazolo[3,4-*b*]pyridines: Synthesis and Biomedical Applications. *Molecules* **2022**, *27*, 2237. [CrossRef] [PubMed]
22. Farahat, A.A.; Samir, E.M.; Zaki, M.Y.; Serya, R.A.; Abdel-Aziz, H.A. Synthesis and in vitro antiproliferative activity of certain novel pyrazolo[3,4-b]pyridines with poten- tial p38α MAPK-inhibitory activity. *Archiv der Pharmazie* **2022**, *355*, 2100302. [CrossRef] [PubMed]
23. Hassan, G.S.; Georgey, H.H.; Mohammed, E.Z.; George, R.F.; Mahmoud, W.R.; Omar, F.A. Mechanistic selectivity investigation and 2D-QSAR study of some new antipro- liferative pyrazoles and pyrazolopyridines as potential CDK2 inhibitors. *Eur. J. Med. Chem.* **2021**, *218*, 113389. [CrossRef] [PubMed]
24. Elewa, M.A.F.; Eldehna, W.M.; Hamdan, A.M.E.; Abd El-kawi, S.H.; El-Kalaawy, A.M.; Majrashi, T.A.; Barghash, R.F.; Abdel-Aziz, H.A.; Hashem, K.S.; Al-Gayyar, M.M.H. WRH-2412 alleviates the progression of hepatocellular carcinoma through regulation of TGF-β/β-catenin/α-SMA pathway. *J. Enz. Inhib. Med. Chem.* **2023**, *38*, 2185761. [CrossRef]
25. Barghash, R.F.; Eldehna, W.M.; Kovalová, M.; Vojáčková, V.; Kryštof, V.; Abdel- Aziz, H.A. One-pot three-component synthesis of novel pyrazolo[3,4-*b*]pyridines as po- tent antileukemic agents. *Eur. J. Med. Chem.* **2022**, *227*, 113952. [CrossRef]
26. Li, Y.; Zhang, J.; Gao, W.; Zhang, L.; Pan, Y.; Zhang, S.; Wang, Y. Insights on structural characteristics and ligand binding mechanisms of CDK2. *Int. J. Mol. Sci.* **2015**, *16*, 9314–9340. [CrossRef]
27. Łukasik, P.; Baranowska-Bosiacka, I.; Kulczycka, K.; Gutowska, I. Inhibitors of cyclin-dependent kinases: Types and their mechanism of action. *Int. J. Mol. Sci.* **2021**, *22*, 2806. [CrossRef]
28. Ramalho, T.C.; Rocha, M.V.; da Cunha, E.F.; Oliveira, L.C.; Carvalho, K.T. Understanding the molecular behavior of organotin compounds to design their effective use as agrochemicals: Exploration via quantum chemistry and experiments. *J. Biomol. Struct. Dyn.* **2010**, *28*, 227–238. [CrossRef]
29. Hammoud, M.M.; Khattab, M.; Abdel-Motaal, M.; Van der Eycken, J.; Alnajjar, R.; Abulkhair, H.S.; Al-Karmalawy, A.A. Synthesis, structural characterization, DFT calculations, molecular docking, and molecular dynamics simulations of a novel ferrocene derivative to unravel its potential antitumor activity. *J. Biomol. Struct. Dyn.* **2023**, *41*, 5199–5216. [CrossRef]
30. de Lima, W.E.A.; Pereira, A.F.; de Castro, A.A.; da Cunha, E.F.F.; Ramalho, T.C. Flexibility in the molecular design of acetylcholinesterase reactivators: Probing representative conformations by chemometric techniques and docking/QM calculations. *Lett. Drug Des. Discov.* **2016**, *13*, 360–371. [CrossRef]
31. Daina, A.; Michielin, O.; Zoete, V. SwissADME: A free web tool to evaluate pharmacokinetics, drug-likeness and medicinal chemistry friendliness of small molecules. *Sci. Rep.* **2017**, *7*, 42717. [CrossRef] [PubMed]
32. Daina, A.; Zoete, V. A boiled-egg to predict gastrointestinal absorption and brain penetration of smallmolecules. *Chem. MedChem.* **2016**, *11*, 1117–1121.

33. Kuriakose, D.; Thumpakara, R.K.; Jesna, A.; Jacob, J.P. Substituent effects in the formation of a few acenaphthenone-2-ylidene ketones and their molecular docking studies and in silico ADME profile. *J. Mol. Struct.* **2021**, *1224*, 129209. [CrossRef]
34. Yoon, S.H.; Kim, S.J.; Kim, I. One-Pot Four-Component Coupling Approach to Polyheterocycles: 6*H*-Furo[3,2-*f*]pyrrolo[1,2-*d*][1,4]diazepine. *J. Org. Chem.* **2020**, *85*, 15082–15091. [CrossRef] [PubMed]
35. Zeng, L.Y.; Liu, T.; Yang, J.; Yang, Y.; Cai, C.; Liu, S. "On-Water" Facile Synthesis of Novel Pyrazolo[3,4-*b*]pyridinones Possessing Anti-influenza Virus Activity. *ACS Comb. Sci.* **2017**, *19*, 437–446. [CrossRef]
36. Kantevari, S.; Chary, M.V.; Vuppalapati, S.V.N. A highly efficient regioselective one-pot synthesis of 2,3,6-trisubstituted pyridines and 2,7,7-trisubstituted tetrahydroquinolin-5-ones using $K_5CoW_{12}O_{40}{\cdot}3H_2O$ as a heterogeneous recyclable catalyst. *Tetrahedron* **2007**, *63*, 13024–13031. [CrossRef]
37. Edmondson, J.M.; Armstrong, L.S.; Martinez, A.O. A rapid and simple MTT-based spectrophotometric assay for determining drug sensitivity in monolayer cultures. *J. Tissue Cult. Methods* **1988**, *11*, 15–17. [CrossRef]
38. Pozarowski, P.; Darzynkiewicz, Z. Analysis of cell cycle by flow cytometry. *Methods Mol. Biol.* **2004**, *281*, 301.
39. Crowley, L.C.; Scott, A.P.; Marfell, B.J.; Boughaba, J.A.; Chojnowski, G.; Waterhouse, N.J. Measuring Cell Death by Propidium Iodide Uptake and Flow Cytometry. *Cold Spring Harb. Protoc.* **2016**, *2016*, 647. [CrossRef]
40. Zhang, J.; Gan, Y.; Li, H.; Yin, J.; He, X.; Lin, L.; Xu, S.; Fang, Z.; Kim, B.W.; Gao, L.; et al. Inhibition of the CDK2 and Cyclin A complex leads to autophagic degradation of CDK2 in cancer cells. *Nat. Commun.* **2022**, *13*, 2835. [CrossRef]
41. Vilar, S.; Cozza, G.; Moro, S. Medicinal chemistry and the molecular operating environment (MOE): Application of QSAR and molecular docking to drug discovery. *Curr. Top. Med. Chem.* **2008**, *8*, 1555–1572. [CrossRef] [PubMed]
42. Scholz, C.; Knorr, S.; Hamacher, K.; Schmidt, B. DOCKTITE, A Highly Versatile Step-by-Step Workflow for Covalent Docking and Virtual Screening in the Molecular Operating Environment. *J. Chem. Inf. Model.* **2015**, *55*, 398–406. [CrossRef] [PubMed]
43. Abdelsalam, E.A.; Abd El-Hafeez, A.A.; Eldehna, W.M.; El Hassab, M.A.; Marzouk, H.M.M.; Elaasser, M.M.; Abou Taleb, N.A.; Amin, K.M.; Abdel-Aziz, H.A.; Ghosh, P.; et al. Discovery of novel thiazolyl-pyrazolines as dual EGFR and VEGFR-2 inhibitors endowed with in vitro antitumor activity towards non-small lung cancer. *J. Enzym. Inhib. Med. Chem.* **2022**, *37*, 2265–2282. [CrossRef] [PubMed]
44. SwissADME. Available online: http://www.swissadme.ch/index.php# (accessed on 10 March 2023).